Development of Particle Scattering Models for Supporting Radiative Transfer Simulations

Lei Bi, Wushao Lin, Xiaoyun Tang,
Zheng Wang, Ruirui Zong, Hejun Xie

Acknowledgement: Ping Yang, George Kattawar, Michael Mishchenko, Fuzhong Weng

Department of Atmospheric Sciences, Zhejiang University, Hangzhou, China

2019.05.01

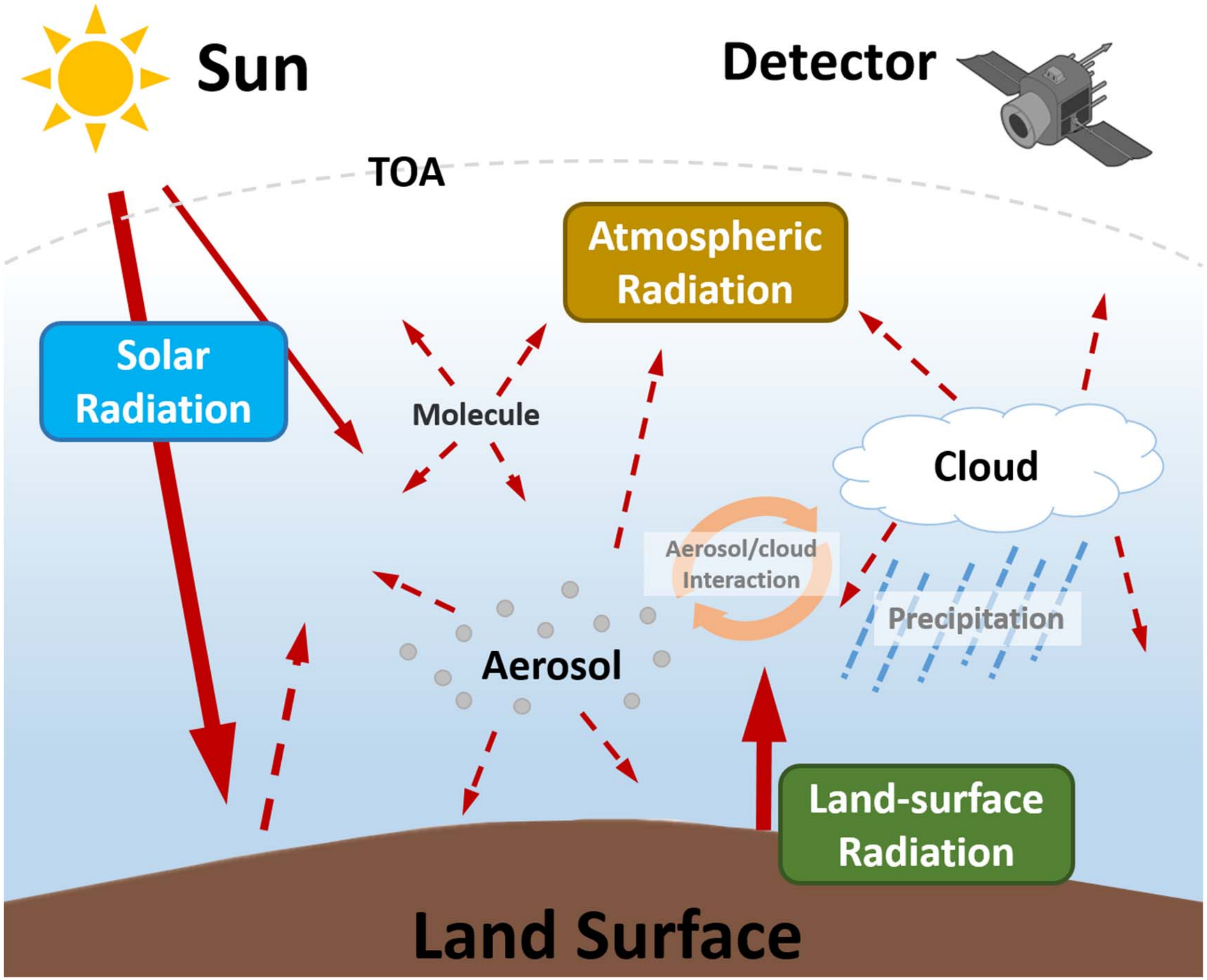
Sun
Detector
TOA
Atmospheric Radiation
Solar Radiation
Molecule
Cloud
Aerosol/cloud Interaction
Precipitation
Aerosol
Land-surface Radiation
Land Surface

Critical Issues

- Tools: Accurate and efficient computational methods to compute the optical properties of arbitrary shaped and inhomogeneous particles
- Physics: Physical mechanism on how particle microphysics affects electromagnetic wave scattering and possible influence on radiative transfer
- Models: Develop "suitable" models for ice crystals and aerosols for atmospheric radiative transfer simulations

Maxwell's Equations

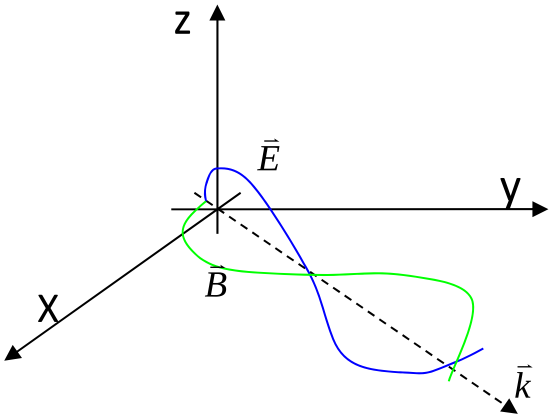

$$\nabla \times \vec{H}(\vec{r}, t) = \frac{\varepsilon}{c} \frac{\partial \vec{E}}{\partial t},$$

$$\nabla \times \vec{E}(\vec{r}, t) = -\frac{\mu}{c} \frac{\partial \vec{H}}{\partial t}$$

Classical theory of light.

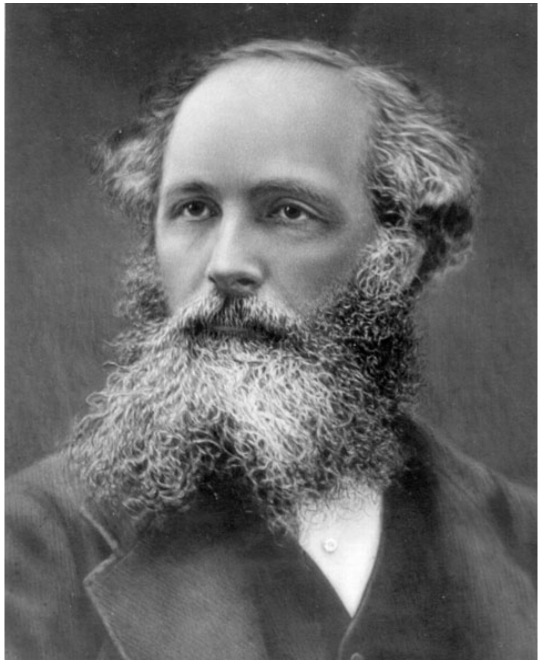

James Clerk Maxwell

Far-field Scattering

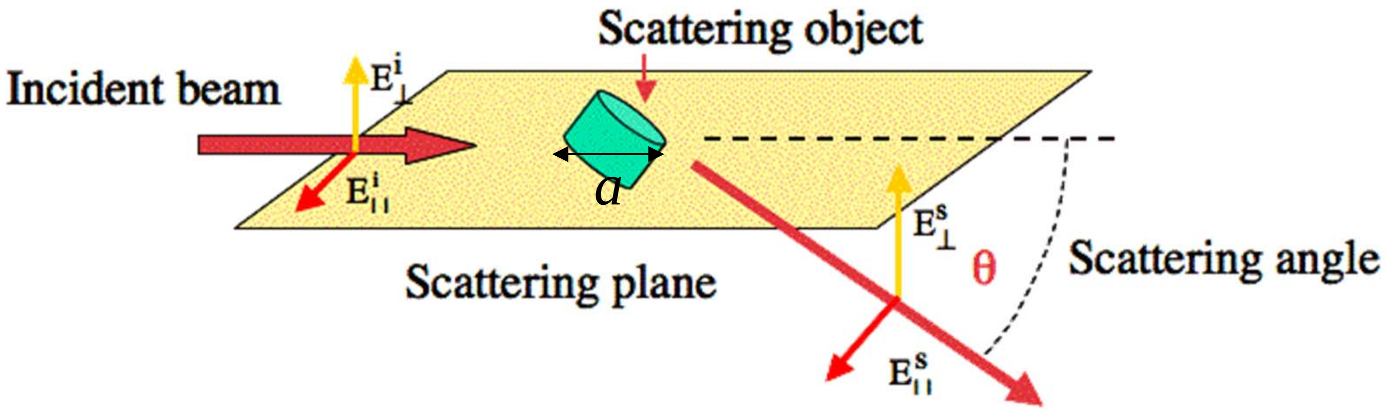

$$k(r-a) >> 1;\ r >> a;\ r >> ka^2/2$$

Observation point

$\vec{r}$

- Amplitude Scattering Matrix

scattered spherical wave

$$\boxed{\begin{pmatrix} E^S_{||} \\ E^S_{\perp} \end{pmatrix} = \frac{e^{ikr}}{-ikr} \begin{pmatrix} S_2 & S_3 \\ S_4 & S_1 \end{pmatrix} \begin{pmatrix} E^i_{||} \\ E^i_{\perp} \end{pmatrix}}$$

Computational Progress

1. **Invariant Imbedding T-matrix**(Bi et al. 2013; Bi and Yang, 2014)

2. **Physical-geometric optics hybrid** (Bi et al., 2011， Bi et al., 2012)

3. **Debye’s series, complex angular momentum** (Bi et al., 2013; Bi et al., 2017; Bi et al., 2019)

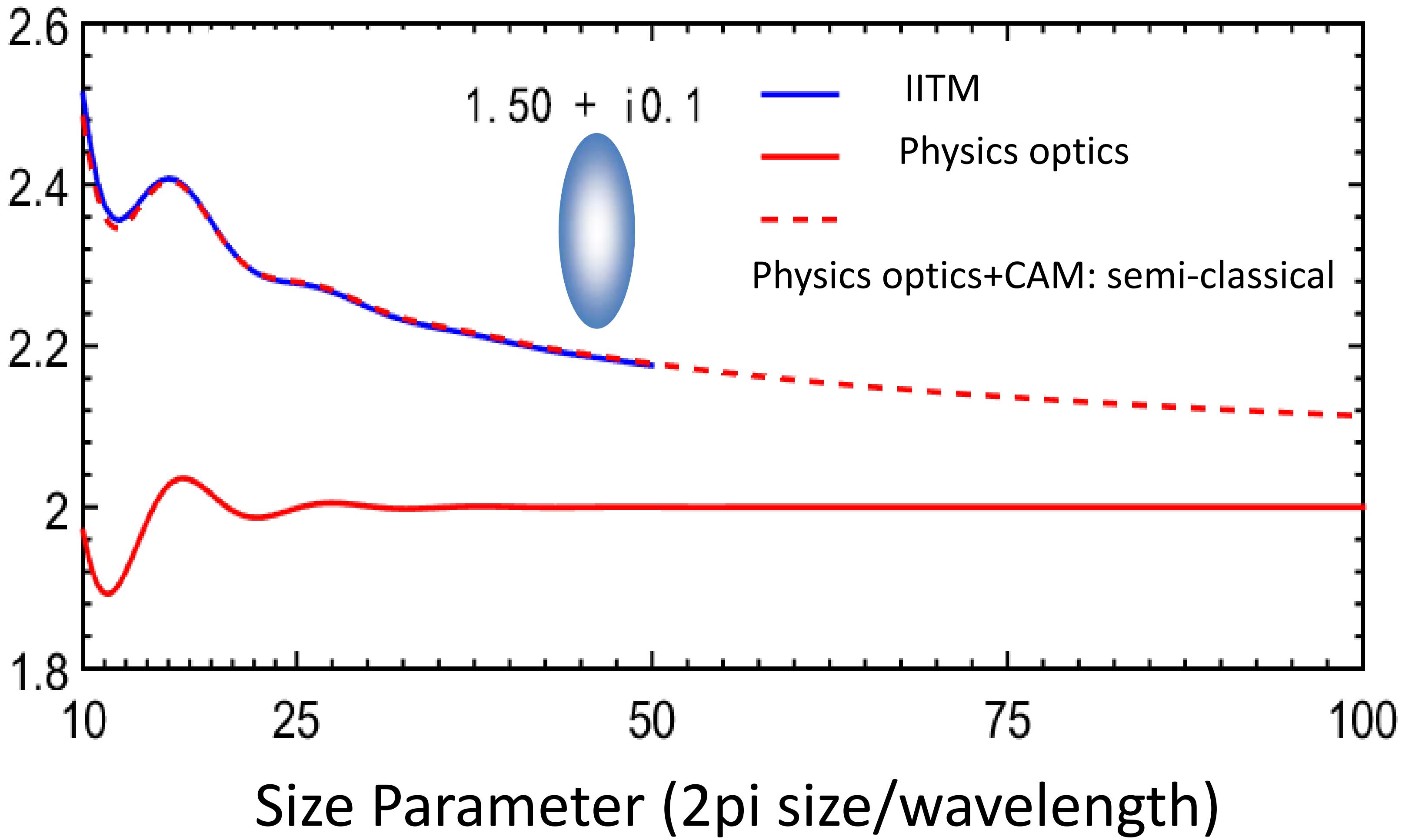
2.6
2.4
2.2
2
1.8
1.50 + i0.1
IITM
Physics optics
Physics optics+CAM: semi-classical
10
25
50
75
100
Size Parameter (2pi size/wavelength)

Invariant Imbedding T-matrix

Distribution of refractive indices

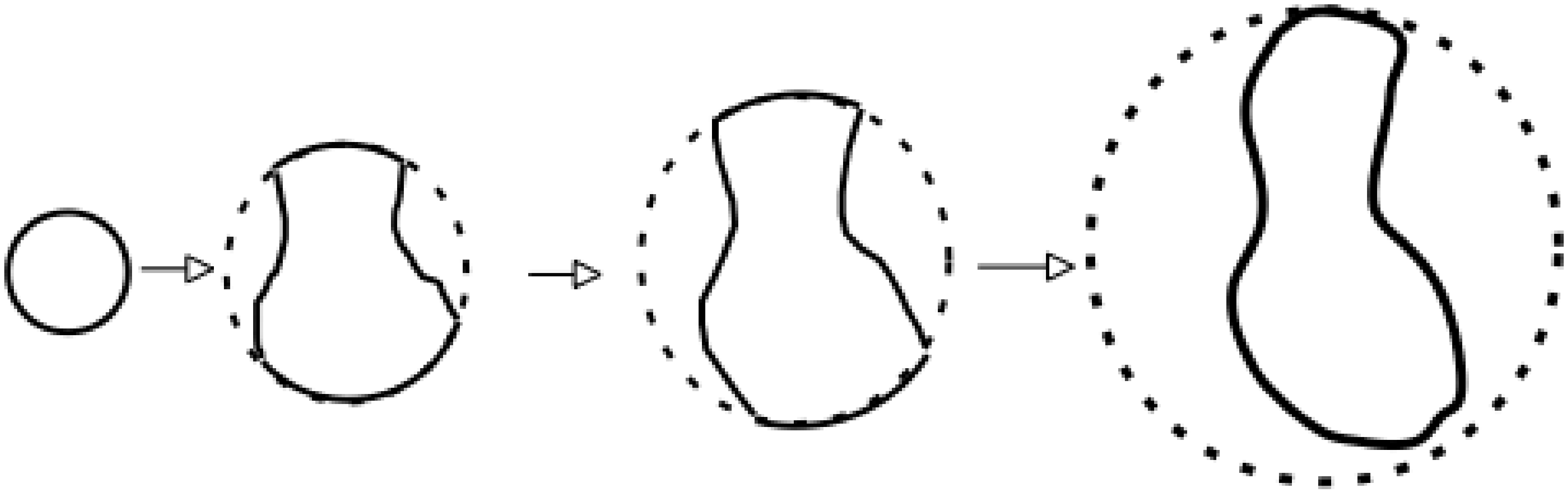

Nonspherical particle = inhomogeneous sphere

=

$$T_{mnmn'}(r+dr)=Q_{11}^{m}(r+dr)+\left[\mathbf{I}+Q_{12}^{m}(r+dr)\right]\left[\mathbf{I}-T_{mnmn'}(r)Q_{22}^{m}(r+dr)\right]^{-1}T_{mnmn'}(r)\left[\mathbf{I}+\tilde{Q}_{12}^{m}(r+dr)\right]$$

Johnson (1988), Bi et al. (2013, 2014)

Arbitrarily Shaped Particles

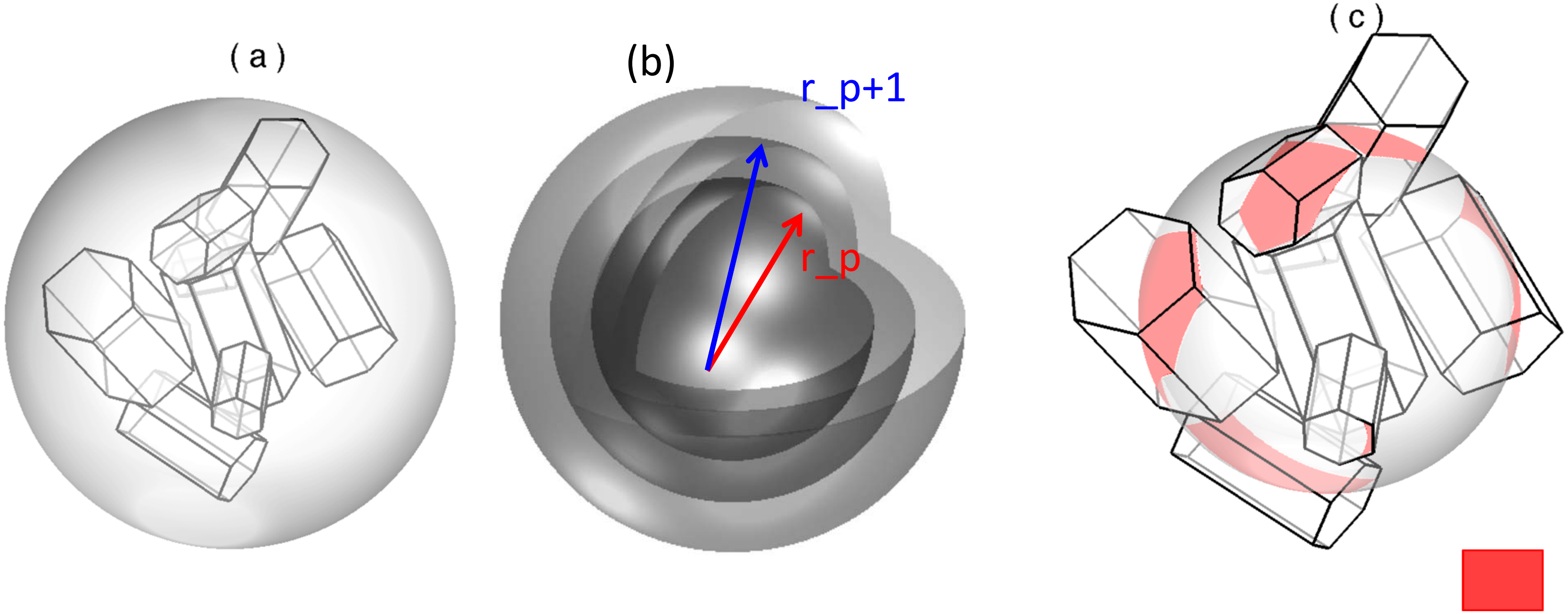

An inhomogeneous sphere Discretize to multi-layered sphere Non-unity refractive index of each spherical surface

Bi, L., and P. Yang, **2014**: Accurate simulation of the optical properties of atmospheric ice crystals with invariant imbedding T-matrix method. *J. Quant. Spectrosc. Radiat. Transfer, 138,17-35.*

Features

- Arbitrary shaped and inhomogeneous particles
- Analytical random orientation average
- Particle size parameter upto geometric-optics domains

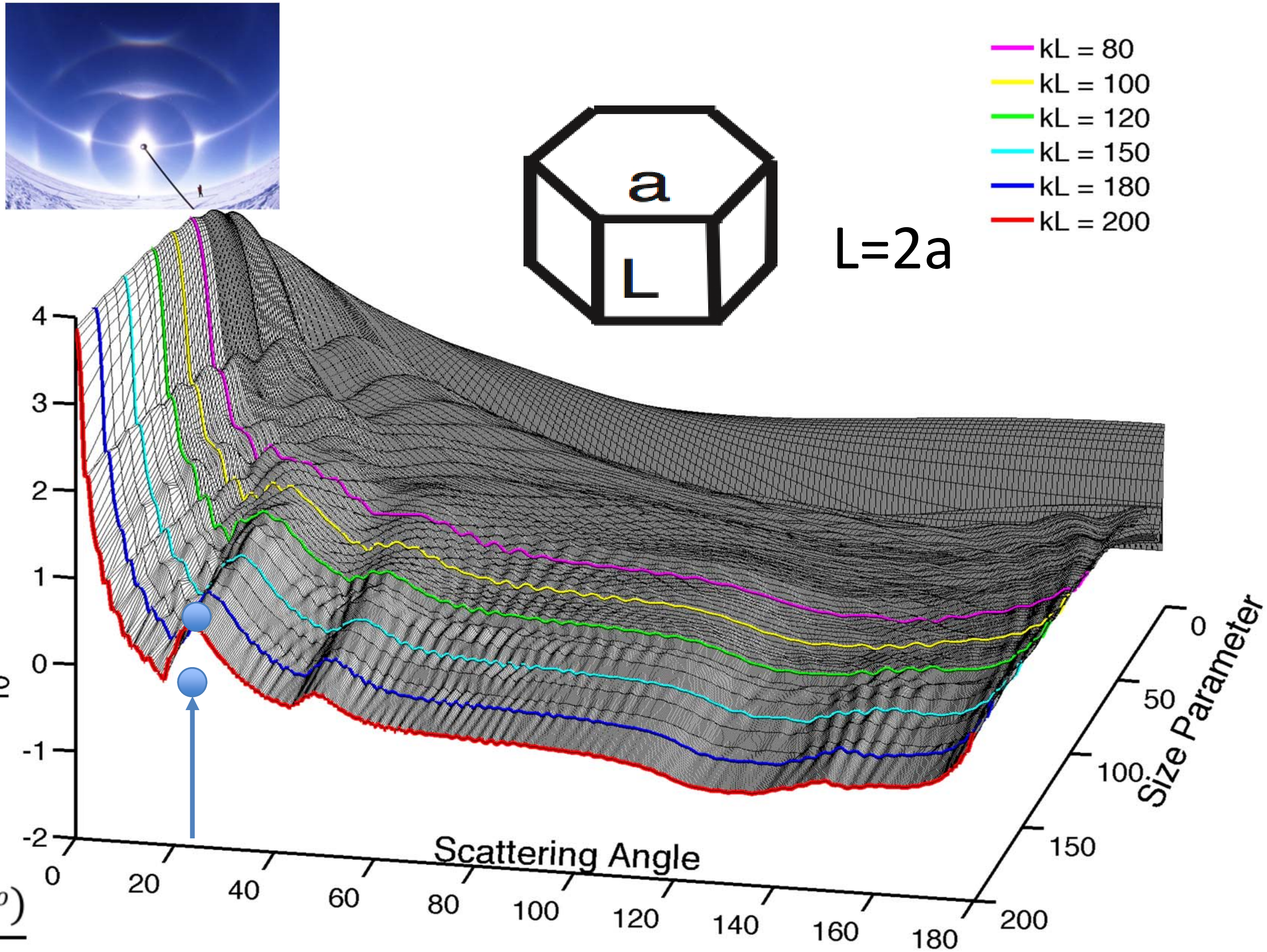
kL = 80
kL = 100
kL = 120
kL = 150
kL = 180
kL = 200
a
L
L=2a
log10(Phase Function)
4
3
2
1
0
-1
-2
Scattering Angle
0
20
40
60
80
100
120
140
160
180
Size Parameter
0
50
100
150
200

$$\frac{P(22^o)}{P_b}$$

Physical geometric-optics Hybrid

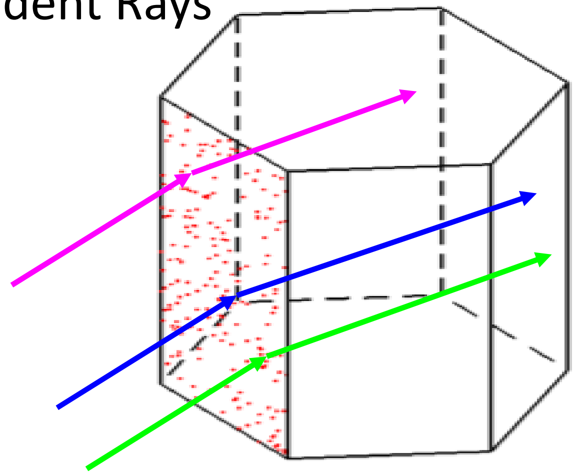

Conventional ray-tracing

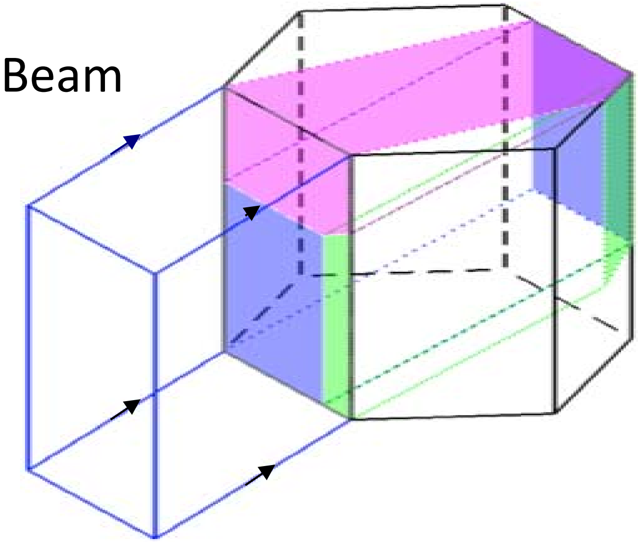

Beam-splitting technique

$$\vec{E}_{sca}(\vec{r}) = \frac{\exp(ikr)}{-ikr}\frac{-ik^3}{4\pi}\iiint_V \left[\tilde{m}^2(\vec{\mathbf{r}}\,') - 1\right]\left\{\vec{E}(\vec{r}\,') - \hat{r}\left[\hat{r}\bullet\vec{E}(\vec{r}\,')\right]\right\}\exp(-ik\vec{r}\bullet\vec{r}\,')d^3\vec{r}\,'$$

Bi, L., P. Yang, G. W. Kattawar, Y. Hu and B. A. Baum, **2012**: Scattering and absorption of light by ice particles: solution by a new physical-geometric optics hybrid method. ***Journal of Quantitative Spectroscopy and Radiative Transfer***, 112, 1492-1508.

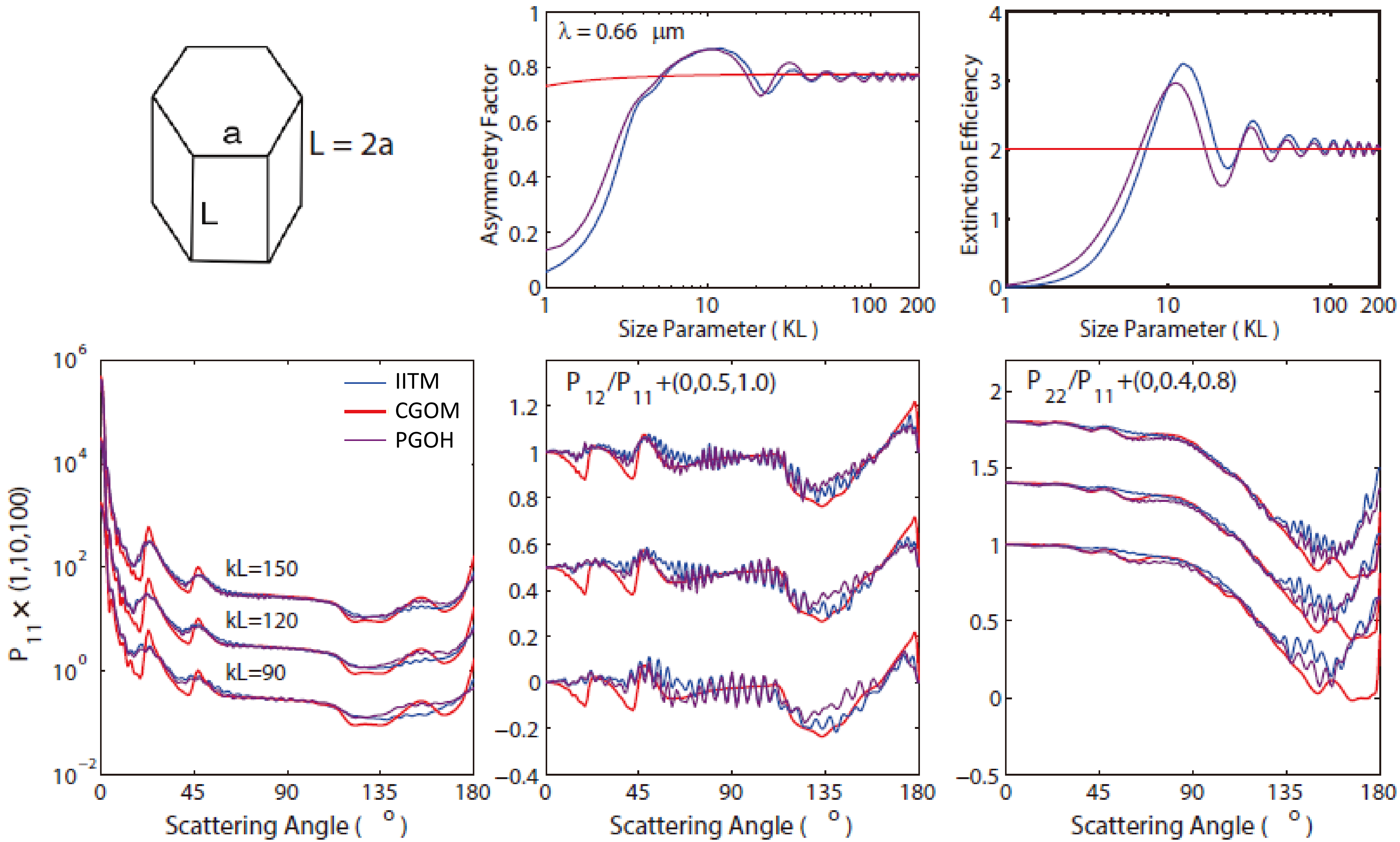

a
L = 2a
L
λ = 0.66 μm
Asymmetry Factor
Size Parameter (KL)
Extinction Efficiency
Size Parameter (KL)
IITM
CGOM
PGOH
kL=150
kL=120
kL=90
P11 × (1,10,100)
Scattering Angle (o)
P12/P11+(0,0.5,1.0)
Scattering Angle (o)
P22/P11+(0,0.4,0.8)
Scattering Angle (o)

Debye's Series

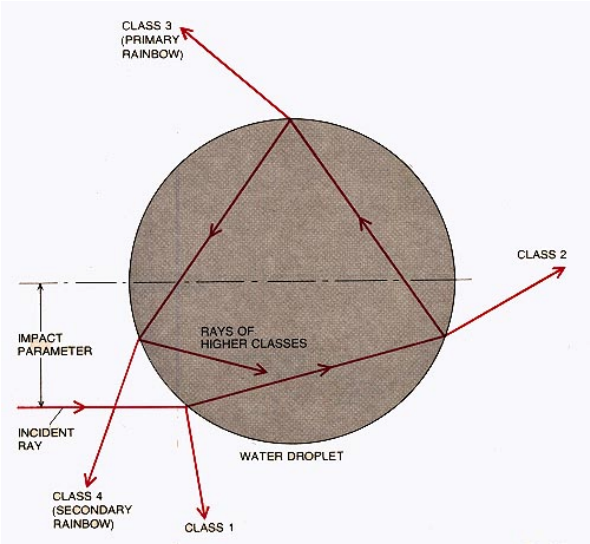

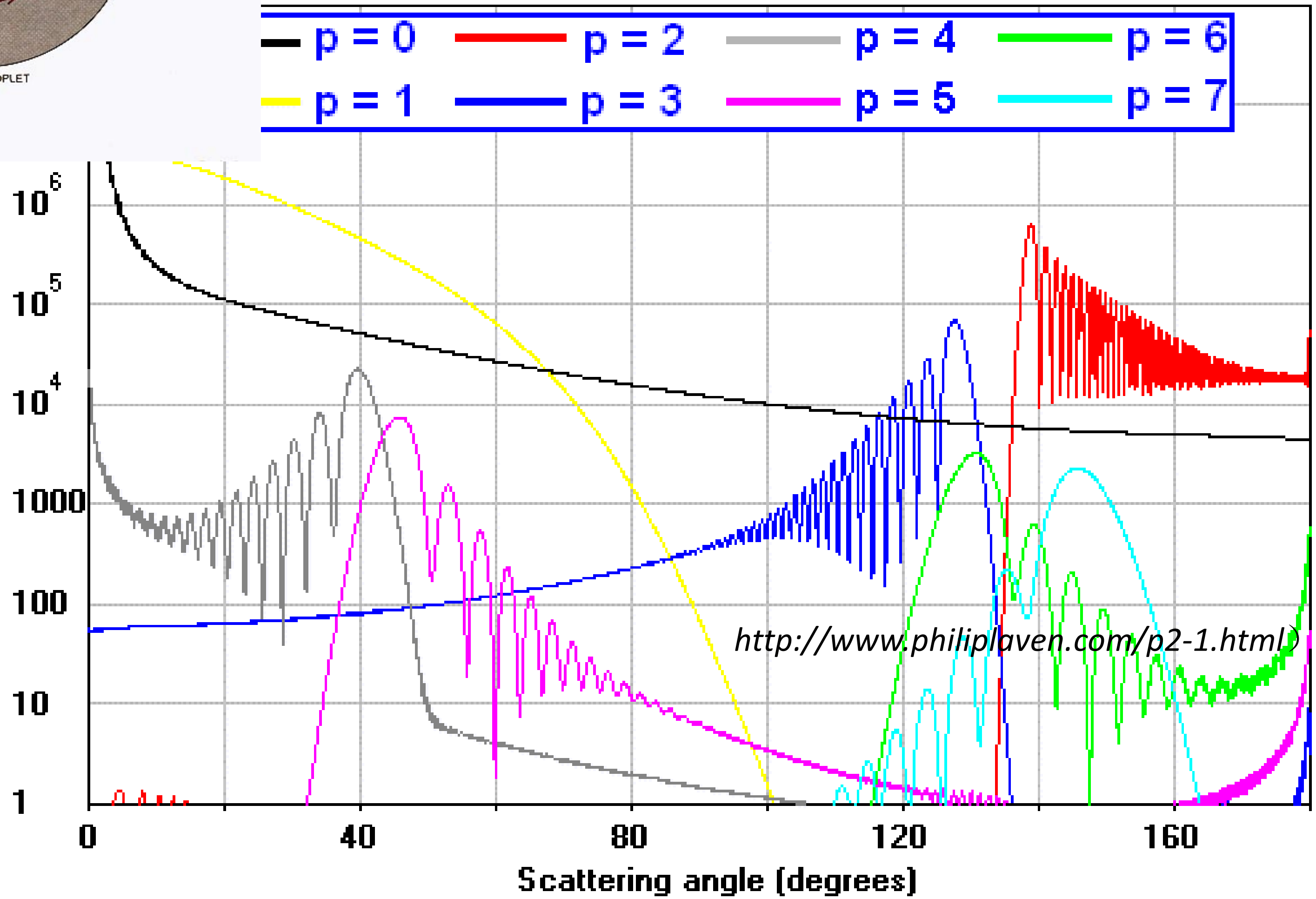

T-matrix Expansion: Debye's Series

$$T = -\frac{1}{2}\left[1 - R_{11} - T_{12}\left(\sum_{n=0}^{\infty}(R_{22})^n\right)T_{21}\right] = -\frac{1}{2}\left[1 - R_{11} - T_{12}\frac{1}{1-R_{22}}T_{21}\right]$$

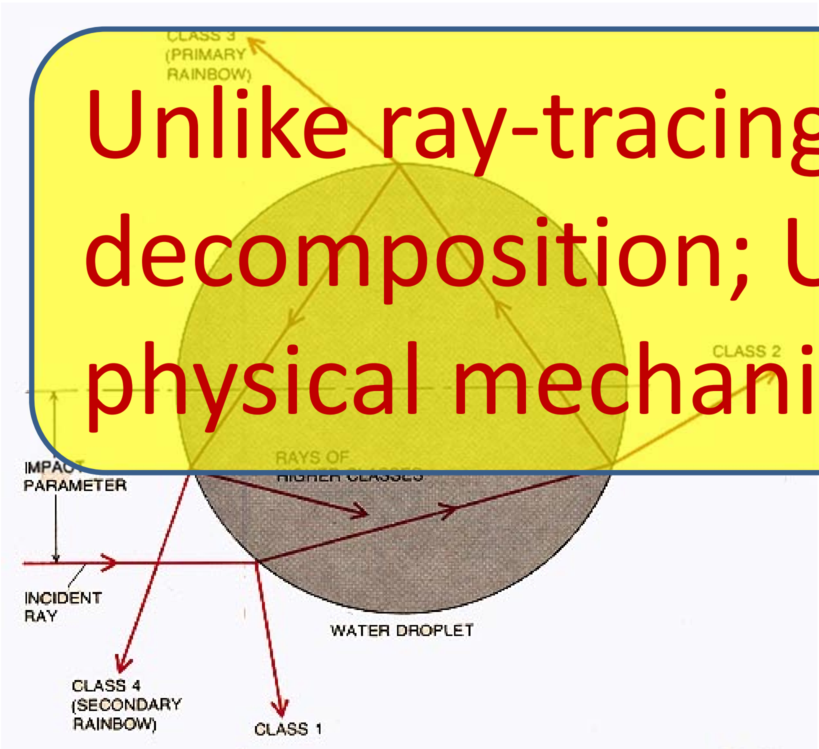

(Debye,1908; Van der Pol and H. Bremmer ,1937;Feng et al,2010)

Unlike ray-tracing, exact decomposition; Understanding physical mechanism

R_{11}: External Reflection

R_{22}: Internal Reflection

T_{21}: Transmission from medium to particle

T_{12}: Transmission from particle to medium

Validated for Convex Nonspherical Particles

Lei Bi, Feng Xu, Gérard Gouesbet， 2018; Phys. Rev. A 98,053809; to be submitted, 2019

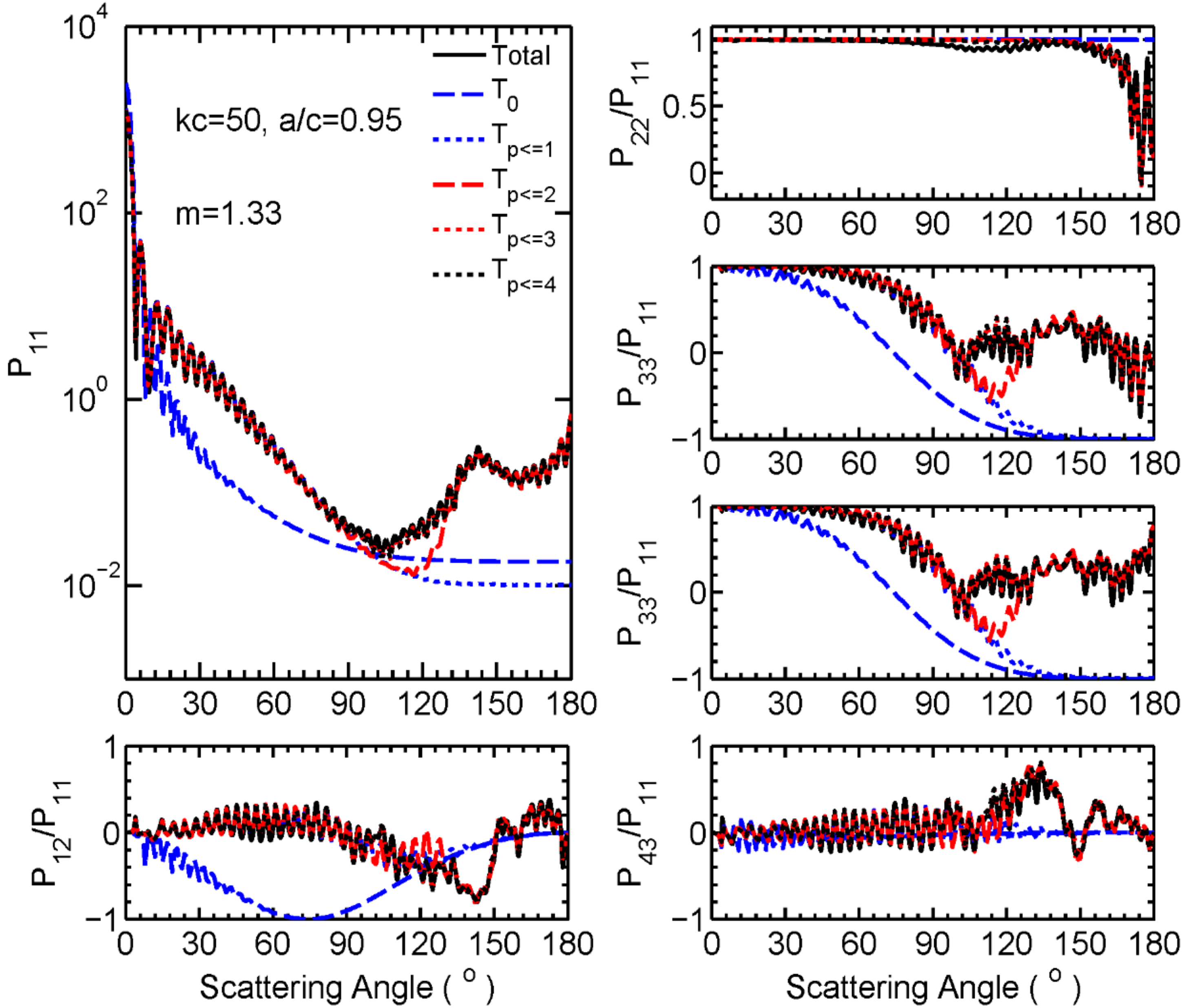

kc=50, a/c=0.95
m=1.33
Total
T_0
$T_{p<=1}$
$T_{p<=2}$
$T_{p<=3}$
$T_{p<=4}$
P_{11}
P_{22}/P_{11}
P_{33}/P_{11}
P_{33}/P_{11}
P_{12}/P_{11}
P_{43}/P_{11}
Scattering Angle (o)
Scattering Angle (o)

Ice Crystal Optical Property Database

Yang, P., **L. Bi**, B. A. Baum, K. N. Liou, G. W. Kattawar, M. I. Mishchenko, and B. Cole, **2013**: *Spectrally consistent scattering, absorption, and polarization properties of atmospheric ice crystals at wavelengths from 0.2 to 100 μm*. ***Journal of the Atmospheric Sciences,*** 70, 330-347.

Bi, L., P. Yang, **2017**: Improved ice particle optical property simulations in the ultraviolet to far-infrared regime. ***Journal of Quantitative Spectroscopy and Radiative Transfer***, 189, 228-237.

Ding, J., **L. Bi**, P. Yang, G. W. Kattawar, F. Weng, Q. Liu, T. Greenwald, 2017: Single-scattering properties of ice particles in the microwave regime: Temperature effect on the ice refractive index with implications in remote sensing. ***Journal of Quantitative Spectroscopy and Radiative Transfer***, 190, 26-37.

Major Aerosol Types

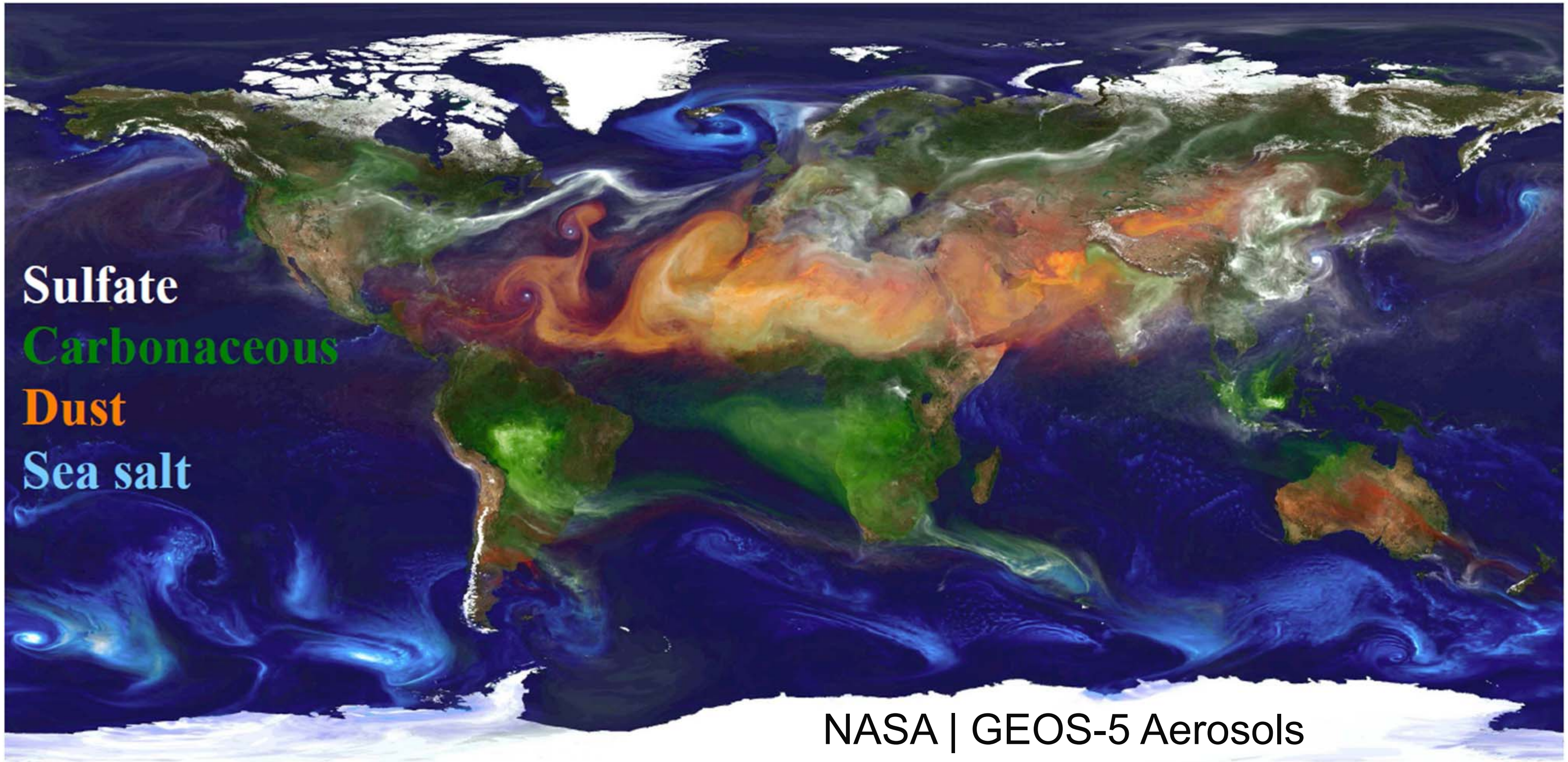

LiDAR Observations

- LiDAR observations are sensitive to the buck-scattering optical properties of a volume element.
- Interpretation: understanding LiDAR signals
- Model constraints: “suitable” models for general radiative transfer simulations

Phase Matrix and Depolarization Ratio

$$\begin{pmatrix} I_s \\ Q_s \\ U_s \\ V_s \end{pmatrix} = \frac{1}{\mathrm{k}^2 r^2} \begin{pmatrix} P_{11} & P_{12} & 0 & 0 \\ P_{12} & P_{22} & 0 & 0 \\ 0 & 0 & P_{33} & P_{34} \\ 0 & 0 & -P_{43} & P_{44} \end{pmatrix} \begin{pmatrix} I_i \\ Q_i \\ U_i \\ V_i \end{pmatrix}$$

Assumption: incident light is 100% polarized **parallel** to the scattering plane

$$\begin{pmatrix} I_i \\ I_i \\ 0 \\ 0 \end{pmatrix} \Rightarrow I_s = (P_{11} + P_{12}) I_i ,\; Q_s = (P_{12} + P_{22}) I_i ,\; U_s = V_s = 0 \Rightarrow \begin{pmatrix} (P_{11} + P_{12}) I_i \\ (P_{12} + P_{22}) I_i \\ 0 \\ 0 \end{pmatrix}$$

$$\begin{aligned} I_s &= (P_{11} + P_{12}) I_i = I_{s\|} + I_{s\perp} \\ Q_s &= (P_{12} + P_{22}) I_i = I_{s\|} - I_{s\perp} \end{aligned} \Longrightarrow \frac{I_{s\perp}}{I_{s\|}} = \frac{P_{11} - P_{22}}{P_{11} + 2P_{12} + P_{22}}$$

Result: scattered light is in general **partially polarized**, i.e. the incident light is **depolarized**

Linear Depolarization Ratio (Random Orientation)

$$\delta(180^o) = \frac{1 - P_{22}/P_{11}}{1 + P_{22}/P_{11}}$$

$$0 \leq \delta \leq 1$$

Zero depolarization ratio cases:

$$\delta = \frac{1 - P_{22}/P_{11}}{1 + 2P_{12}/P_{11} + P_{22}/P_{11}}$$

$$\delta(180^o) = \frac{1 - P_{22}/P_{11}}{1 + P_{22}/P_{11}}$$

Single-scattering by water droplets in water clouds

Nonspherical water droplets in rain with axial incidence

Incident Beam

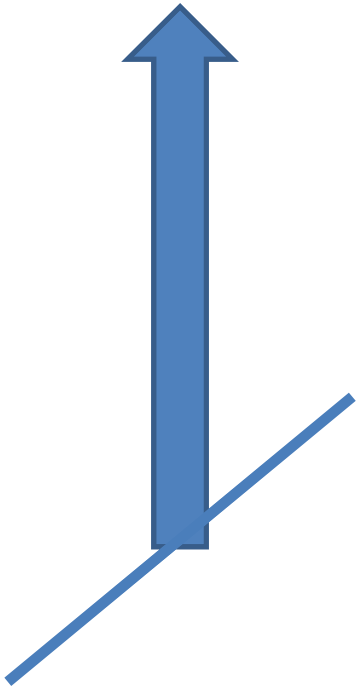

Backscattered Beam

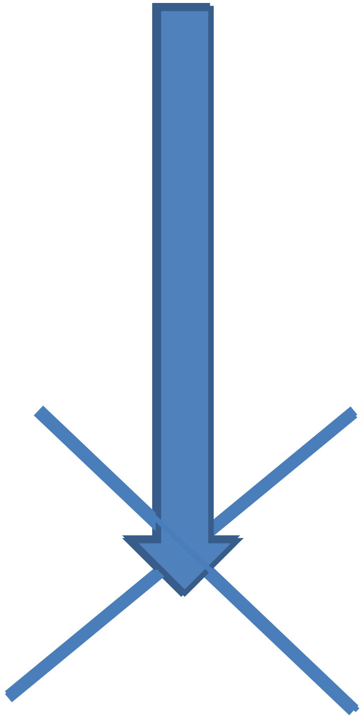

$$\delta(180^\circ) = 100\%$$

Size Distribution

$$\delta = \frac{1 - \int_{r_{\min}}^{r_{\max}} P_{22,180^\circ}(r) C_{sca}(r) \frac{dN}{dr} dr \Big/ \int_{r_{\min}}^{r_{\max}} P_{11,180^\circ}(r) C_{sca}(r) \frac{dN}{dr} dr}{1 + \int_{r_{\min}}^{r_{\max}} P_{22,180^\circ}(r) C_{sca}(r) \frac{dN}{dr} dr \Big/ \int_{r_{\min}}^{r_{\max}} P_{11,180^\circ} C_{sca}(r) \frac{dN}{dr} dr}$$

$$\frac{dN}{dr} = \frac{N_0}{\sqrt{2\pi} r \log(\sigma) \ln(10)} \exp\left\{ -\frac{1}{2} \left[\frac{\log(r) - \log(r_m)}{\log(\sigma)} \right]^2 \right\}$$

Backscatter Lidar Ratio

$$S = \frac{\int_{r_{\min}}^{r_{\max}} C_{ext}(r) \frac{dN}{dr} dr}{P_{11,180^\circ} \int_{r_{\min}}^{r_{\max}} C_{sca}(r) \frac{dN}{dr} dr}$$

How to model particle shapes?

Super-spheroidal Space

$$\left(\frac{x}{a}\right)^{2/n}+\left(\frac{y}{a}\right)^{2/n}+\left(\frac{z}{c}\right)^{2/n}=1$$

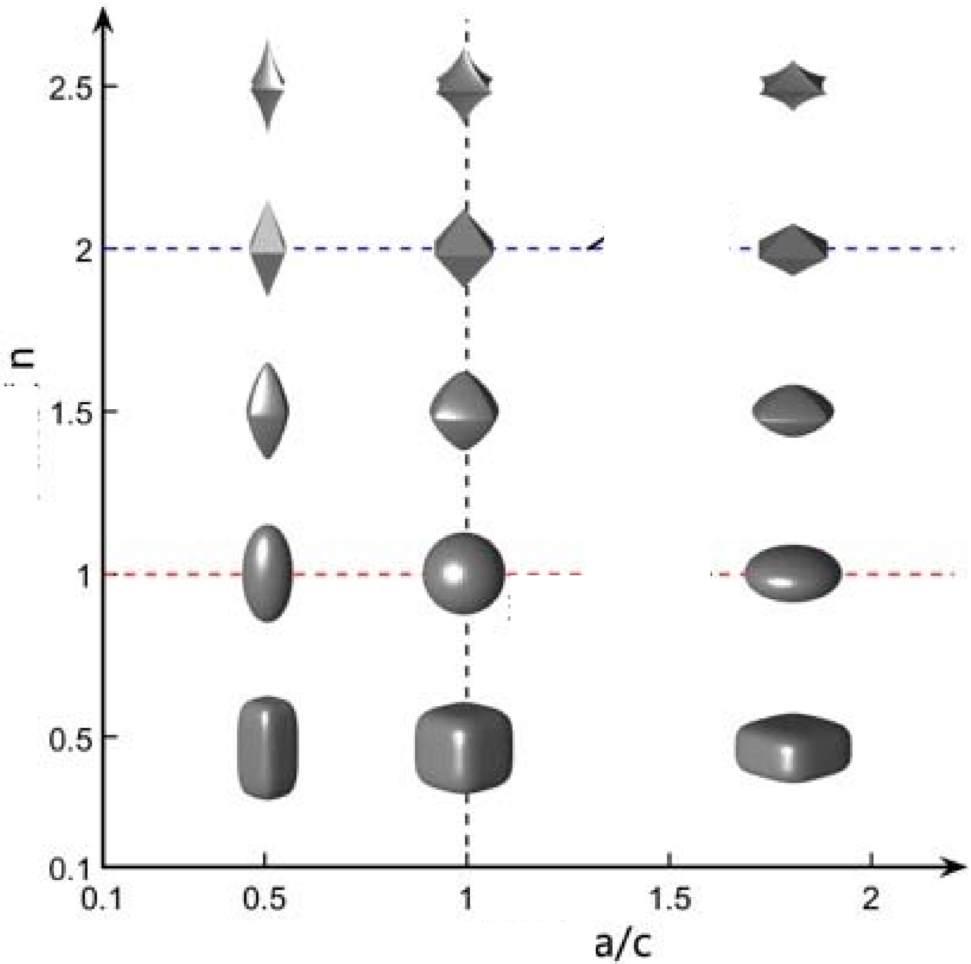

Feldspar

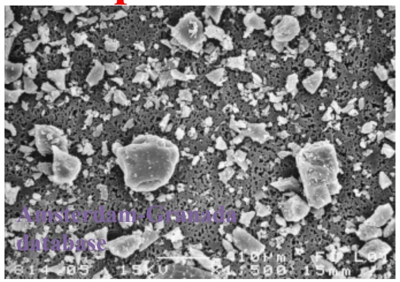

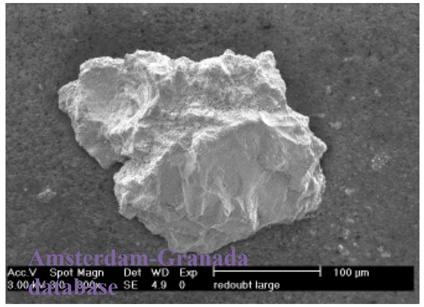

Volcanic ash

n=0.15

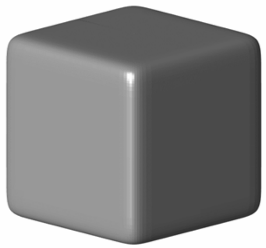

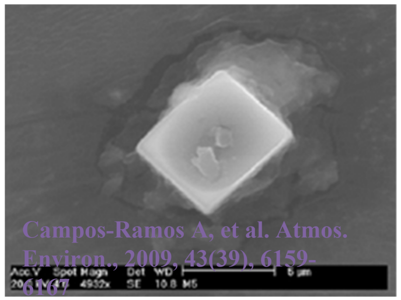

Sodium chloride

Sea salt

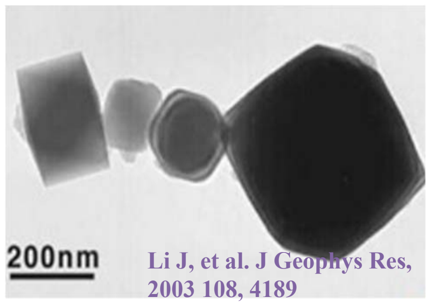

Nearly spherical Particles show quite different depolarization features in aerosol refractive index regime

Spheroids, Refractive Index: 1.55+i0.003

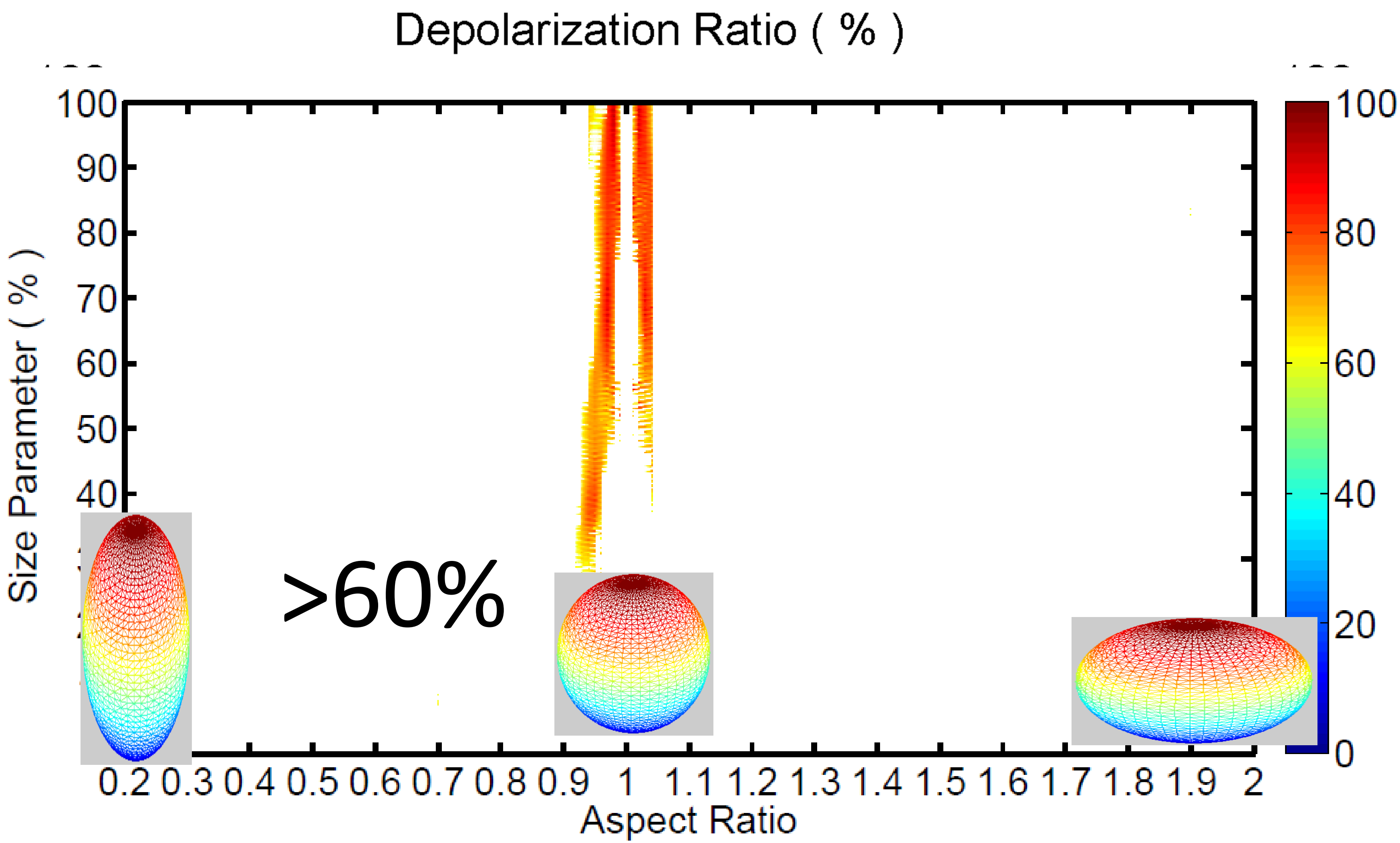

First reported by Mishchenko, M. I., and J. W. Hovenier(1995) at this refractive index

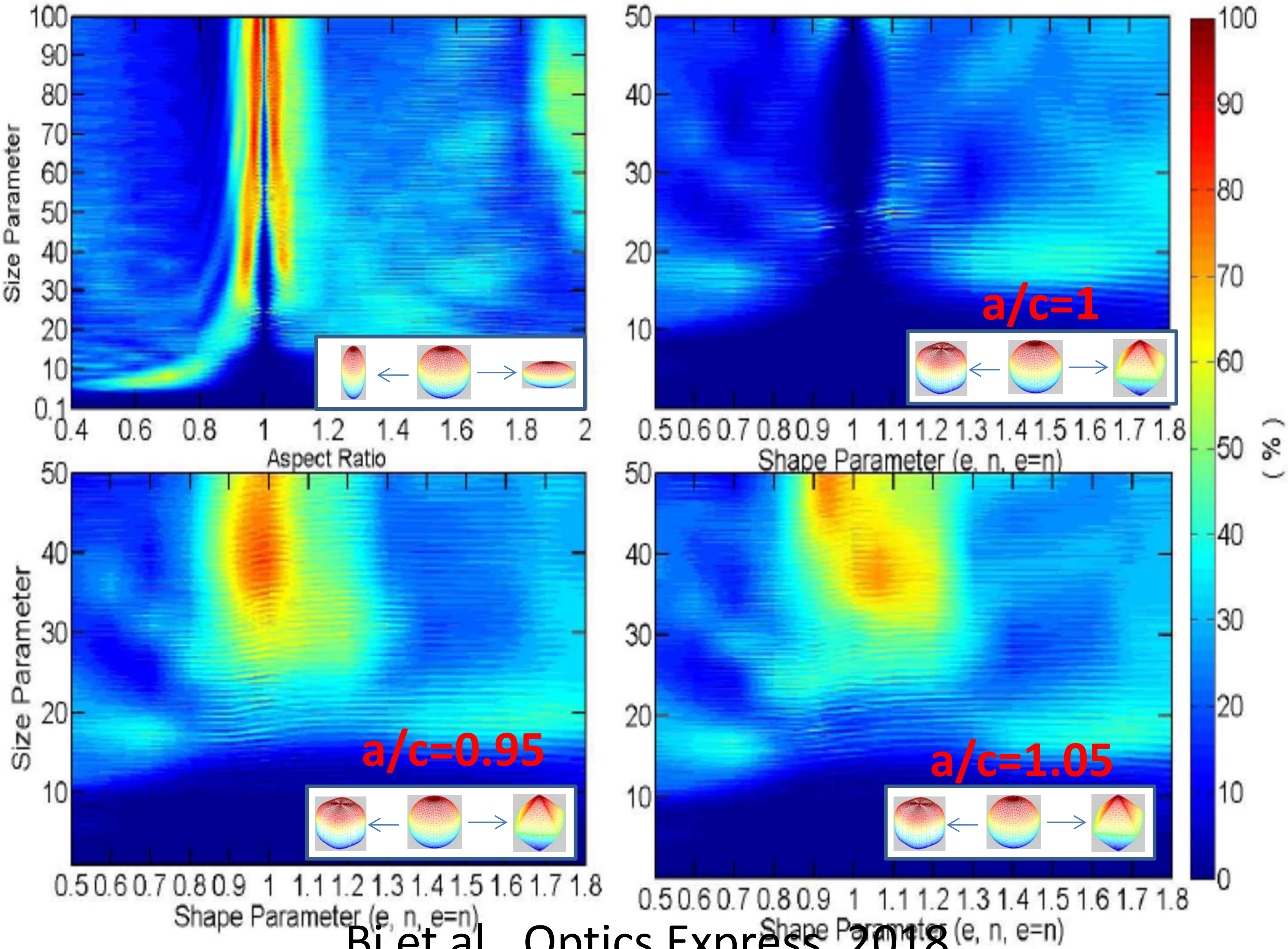

Bi et al., Optics Express, 2018

Refractive Indices at 532 nm

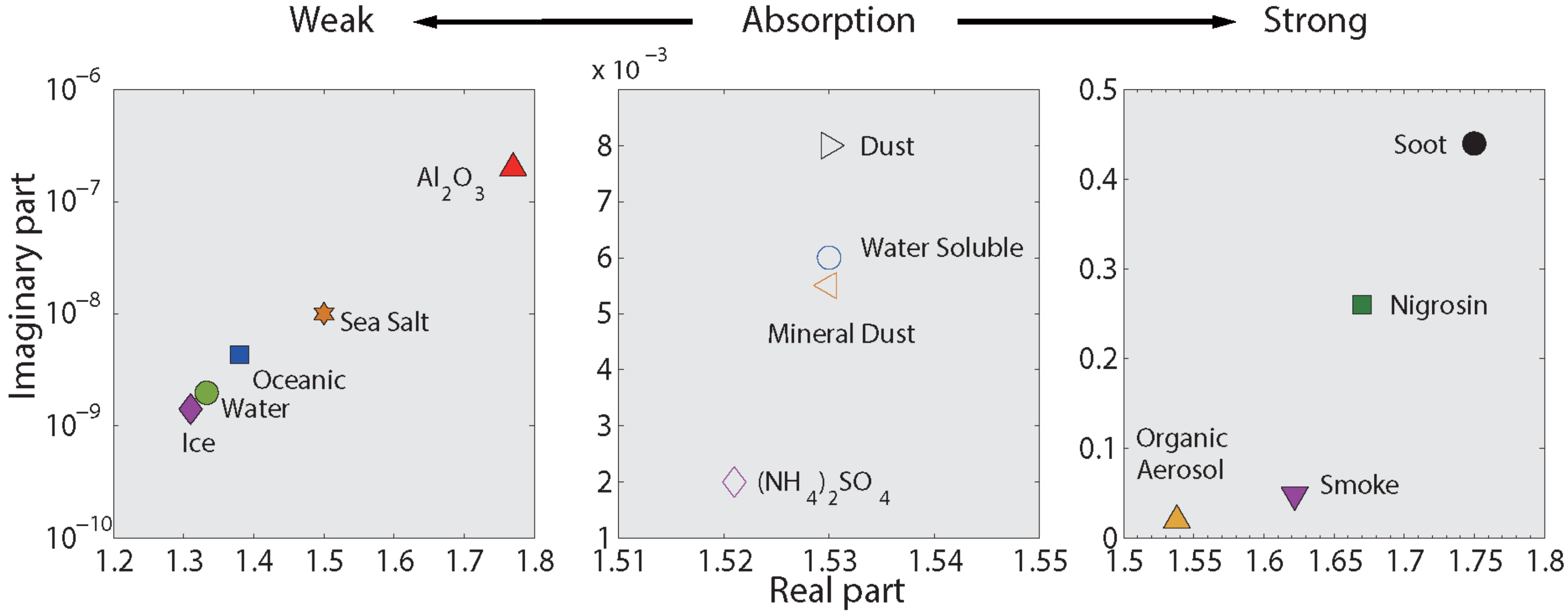

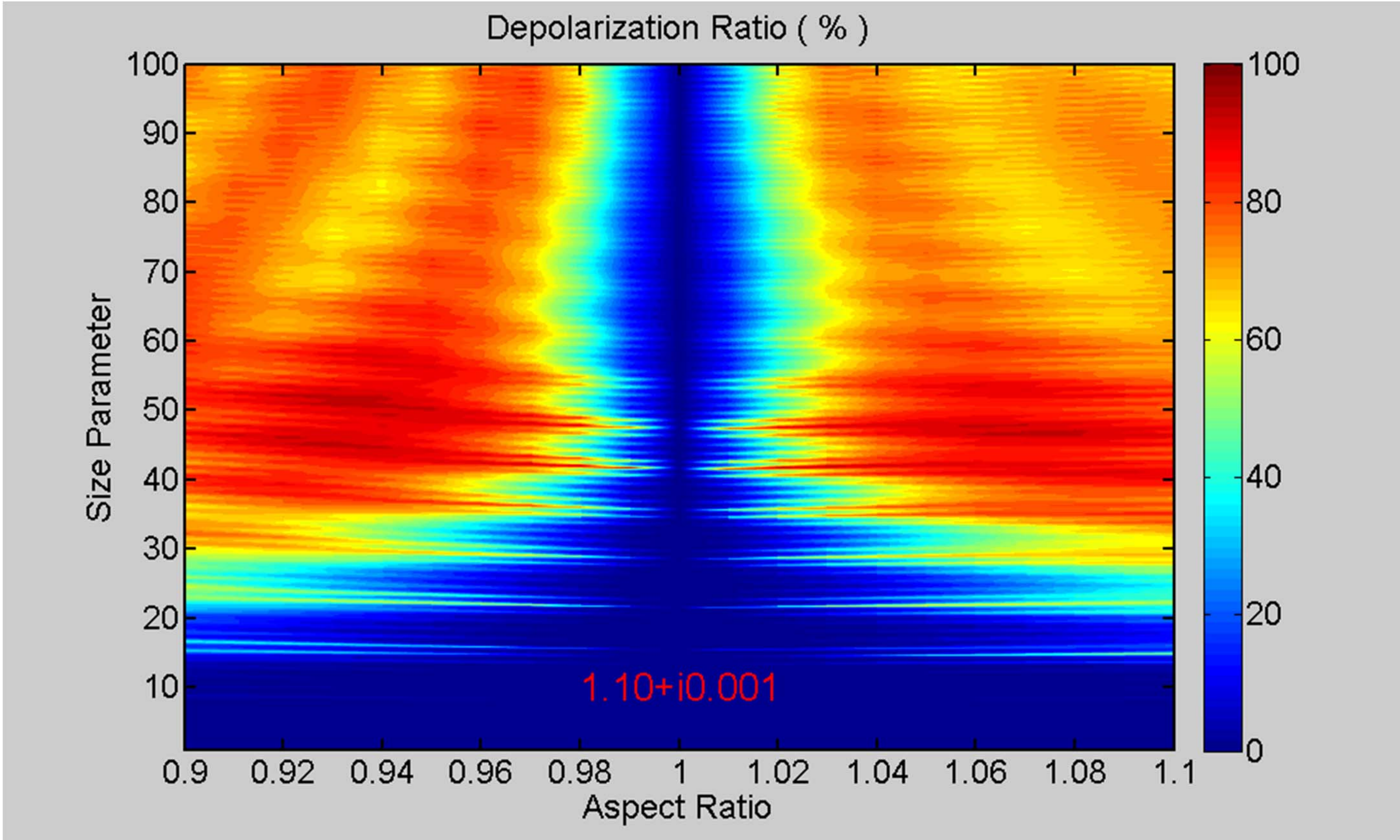
Depolarization Ratio (%)
Size Parameter
Aspect Ratio
100
90
80
70
60
50
40
30
20
10
0.9
0.92
0.94
0.96
0.98
1
1.02
1.04
1.06
1.08
1.1
1.10+i0.001
100
80
60
40
20
0

Different Physical Origins obtained from Debye's series

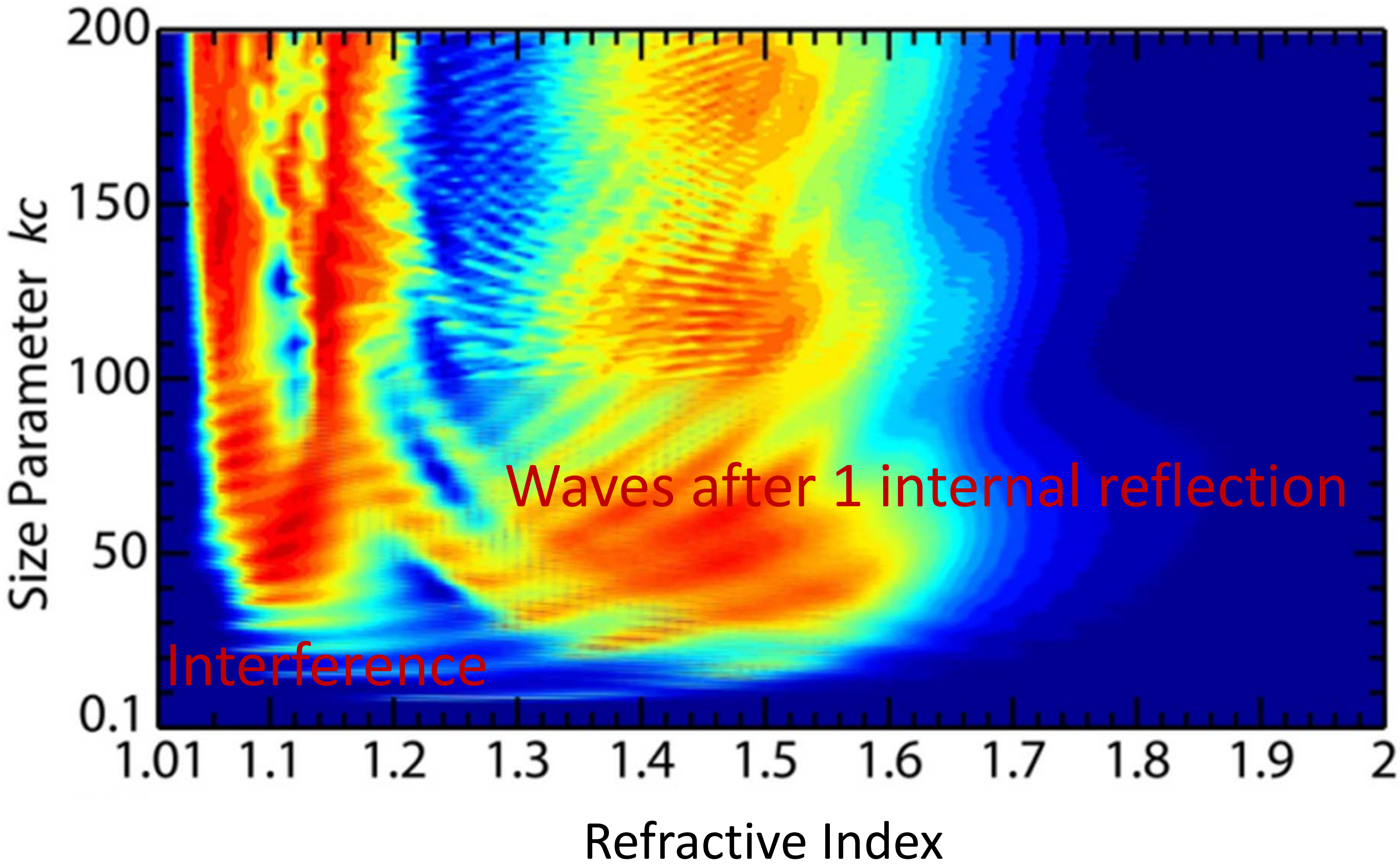

Lei Bi, Feng Xu, Gérard Gouesbet， 2018； Phys. Rev. A 98,053809;

CALIPSO DATA (2012)

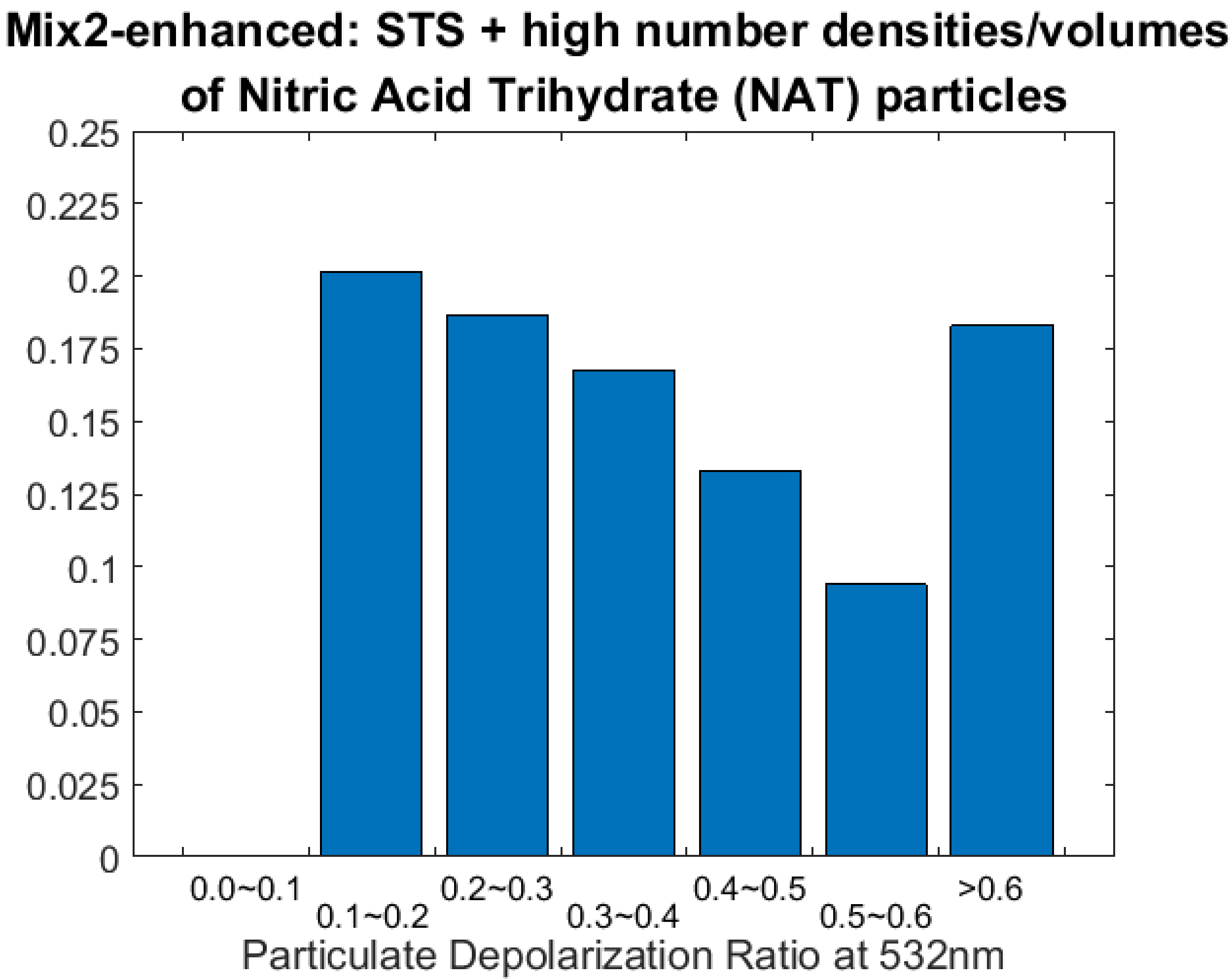

Polar Stratospheric Cloud (PSC) detection descried in (Pitts et al, 2009)

Dust optical modeling

Why more freedom is useful?

S=average projected area
V=volume of a particle

$$\mathrm{SI} = \frac{3V}{4\pi(S/\pi)^{3/2}}$$

SI=1 for a sphere

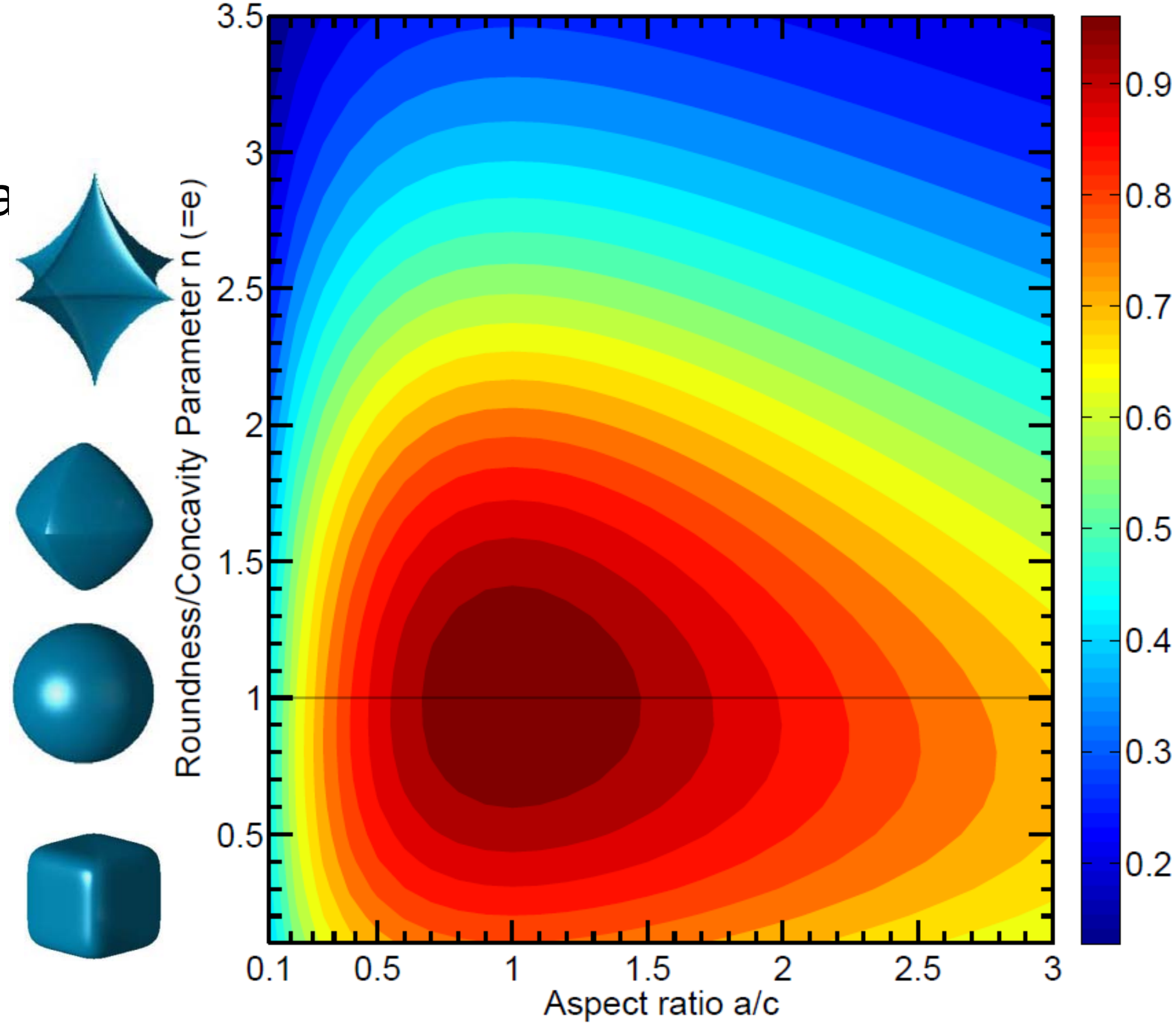

Advantage of SI

- If two nonspherical particles have the same shape index (SI), they have identical volume and projected area.

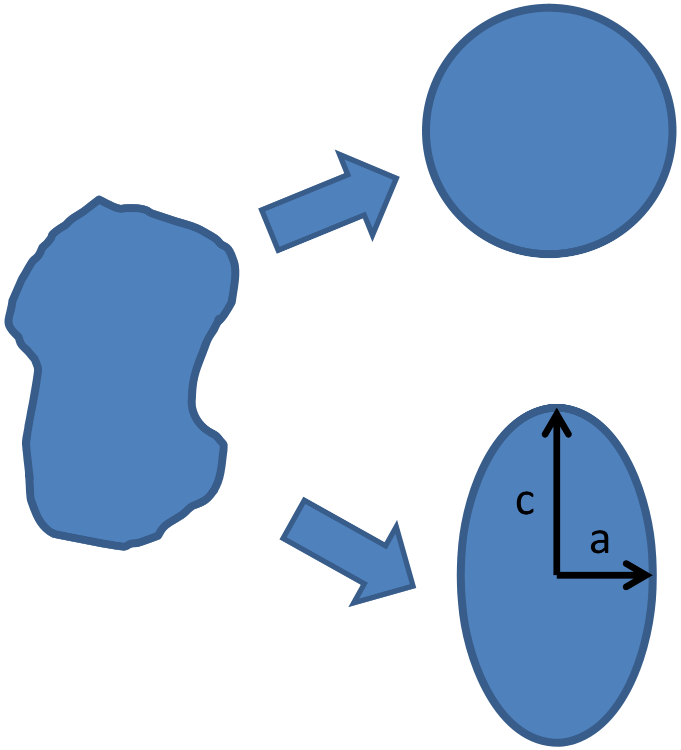

Volume equivalent， surface area？

Surface area equivalent， volume？

Volume equivalent， surface area？

Surface area equivalent， volume？

Stereogrammetry

SI=0.67

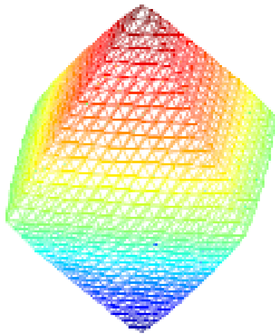

volume, projected area, aspect ratio

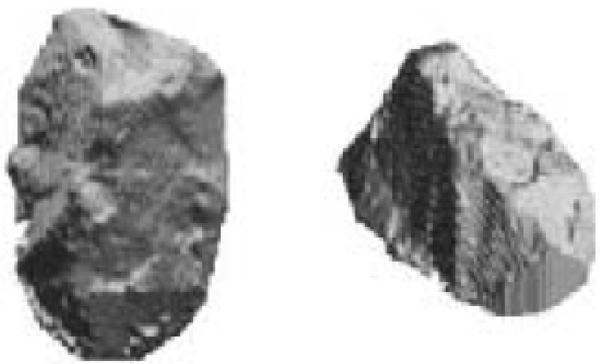

SI=0.82

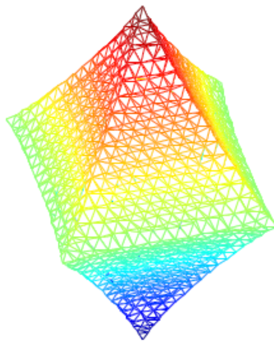

(Image from Lindqvist, et al., 2014)

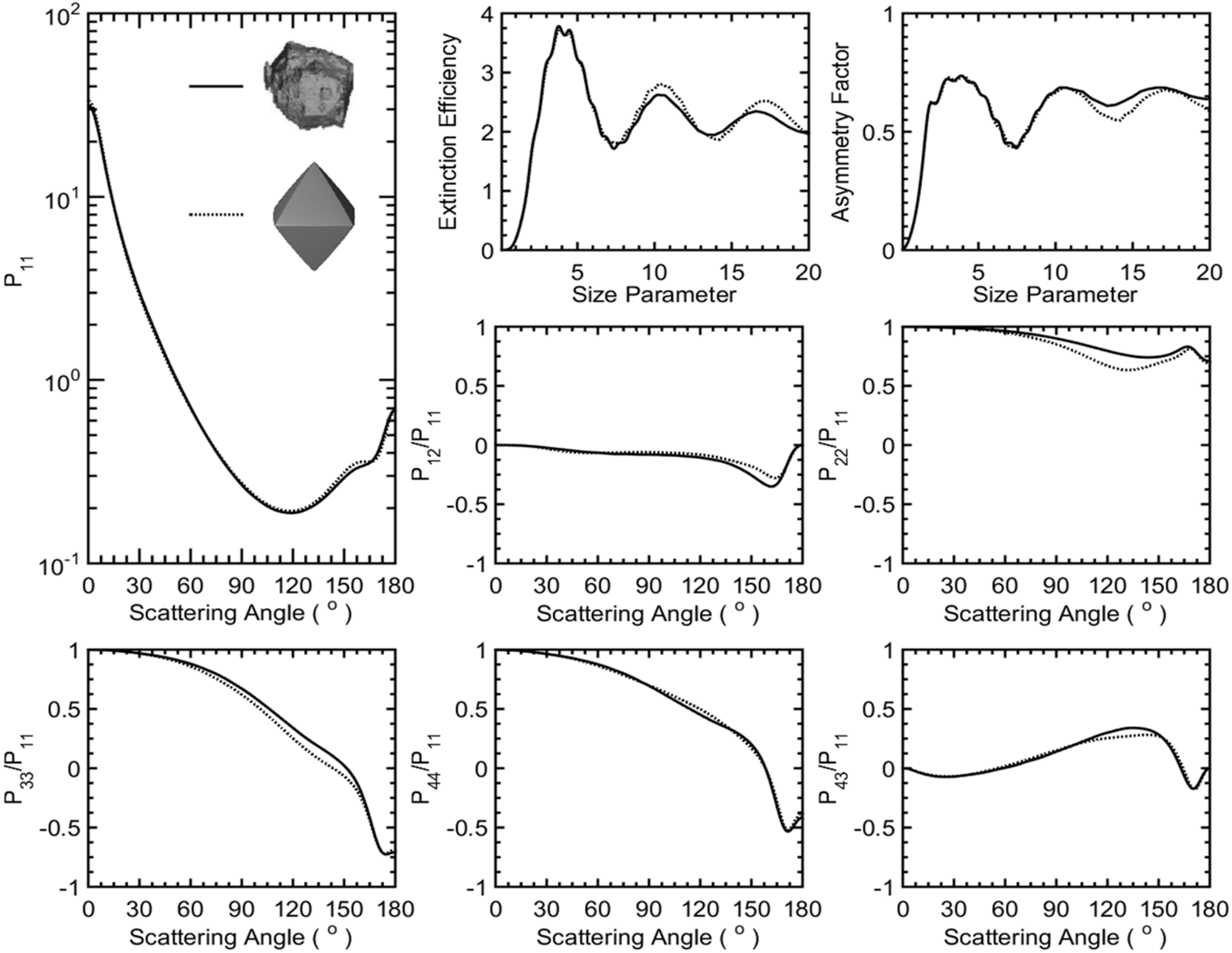

P11
Scattering Angle (o)
Extinction Efficiency
Size Parameter
Asymmetry Factor
P12/P11
P22/P11
P33/P11
P44/P11
P43/P11

Comparison with Laboratory Measuements

Table 1

Summary of the Samples Investigated in this Study

Sample	r_{eff}/μm	v_{eff}	Re(m)	Im(m)
Allende	0.8	3.3	1.65	0.001
Feldspar*	1.0	1.0	1.50–1.60	0.001–0.00001
Red clay*	1.5	1.6	1.50–1.70	0.001–0.00001
Green clay*	1.55	1.4	1.50–1.70	0.001–0.00001
Quartz	2.3	2.3	1.54	0
Martian analog palagonite	4.5	7.3	1.50	0.001–0.0001
Loess*	3.9	2.6	1.50–1.70	0.001–0.00001
Sahara*	8.2	4.0	1.50–1.70	0.001–0.00001
Forsterite (initial)	1.8	5.4	1.63	0
Forsterite (small)	1.3	3.1	1.63	0
Forsterite (washed)	3.3	4.7	1.63	0
Olivine (S)	1.3	1.8	1.62	0.00001
Olivine (M)	2.6	5.0	1.62	0.00001
Olivine (L)	3.8	3.7	1.62	0.00001
Olivine (XL)	6.3	6.8	1.62	0.00001
Volcanic ash (El Chichon)	3.2	5.4	1.50–1.60	0.001
Volcanic ash (Pinatubo)	3.0	12.3	1.50–1.60	0.001–0.00001
Volcanic ash (Lokon)	7.1	2.6	1.50–1.60	0.001–0.00001
Volcanic ash (Mnt. St. Helens)	4.1	9.5	1.48–1.56	0.0018
Volcanic ash (Redoubt A)	4.1	9.7	1.48–1.56	0.0018
Volcanic ash (Redoubt B)	6.4	7.6	1.48–1.56	0.0018
Volcanic ash (Spurr Ashton)	2.7	4.9	1.48–1.56	0.0018–0.02
Volcanic ash (Spurr Gunsight)	3.5	8.2	1.48–1.56	0.0018–0.02
Volcanic ash (Spurr Ahchorage)	4.8	8.8	1.48–1.56	0.0018–0.02
Volcanic ash (Spurr Stop 33)	14.4	6.6	1.48–1.56	0.0018–0.02

Note. The r_{eff} is the effective radius; v_{eff} is the variance; Re(m) and Im(m) are the real part and the imaginary part of the estimated refractive index, respectively.
*These samples have been investigated in Merikallio et al., (2011).

25 Aerosol Samples from the Amsterdam-Granda Light Scattering Database (Voten et al., 2006; Muñoz et al., 2012)

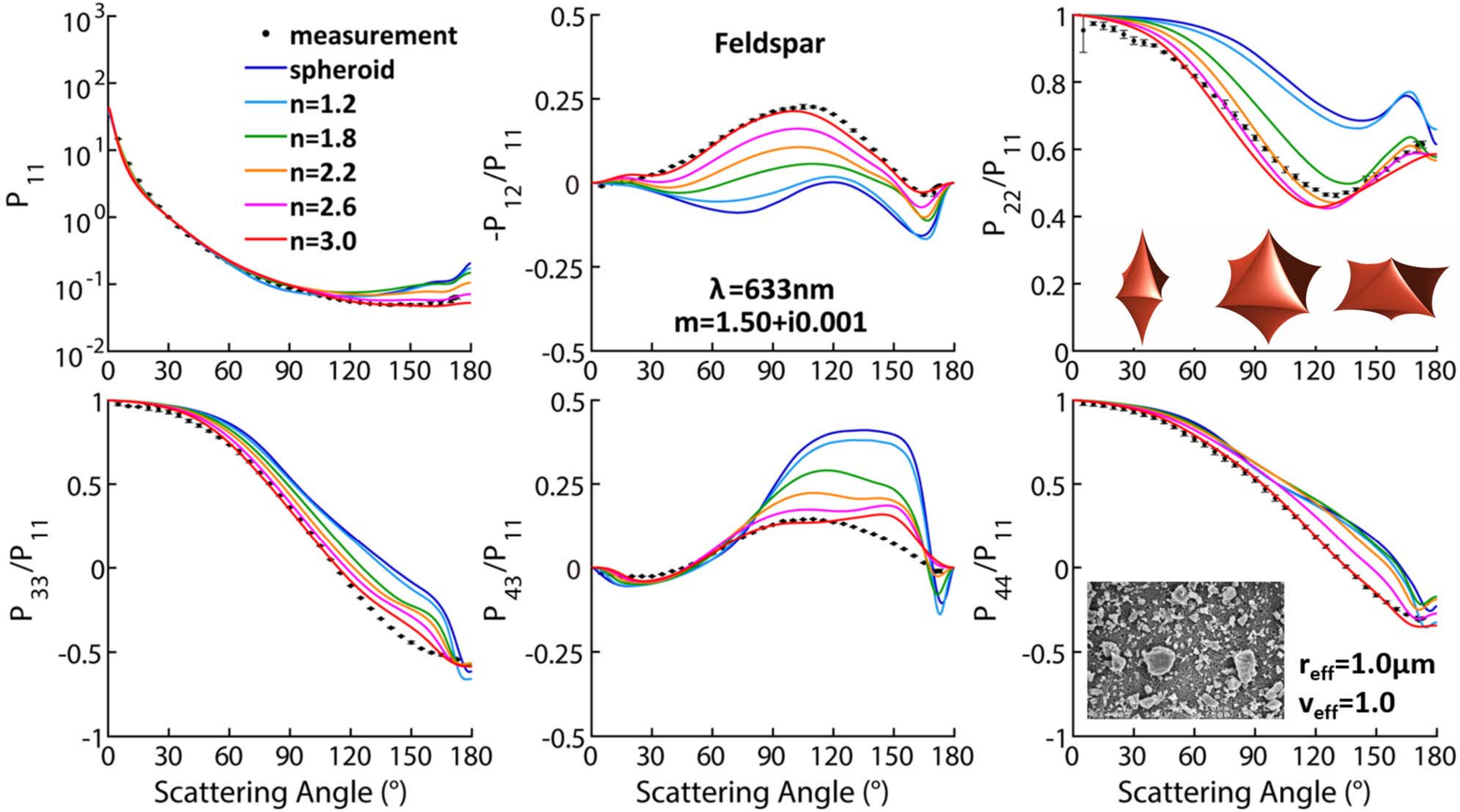

Lin, et al. JGR (2018)

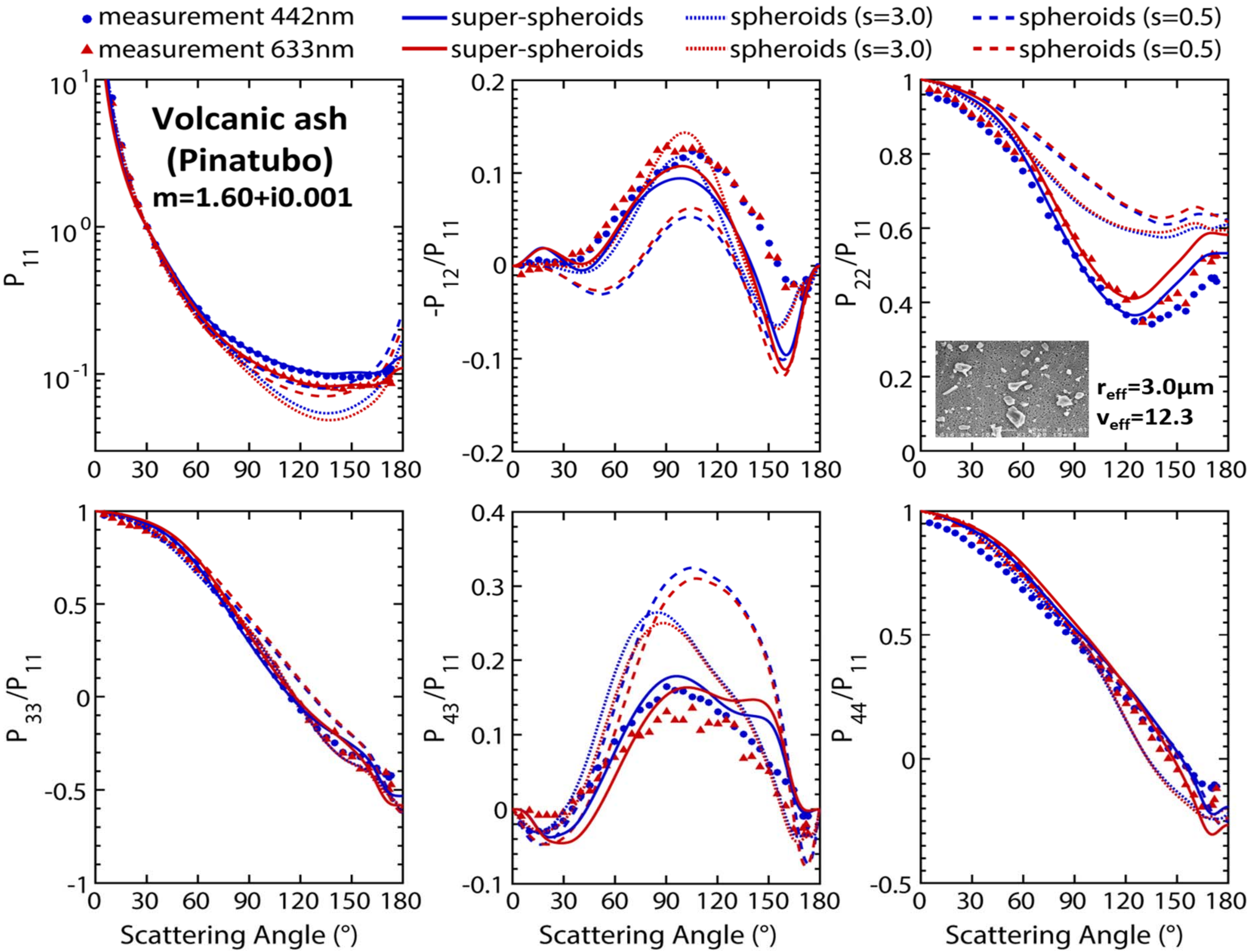
measurement 442nm
measurement 633nm
super-spheroids
super-spheroids
spheroids (s=3.0)
spheroids (s=3.0)
spheroids (s=0.5)
spheroids (s=0.5)
Volcanic ash
(Pinatubo)
m=1.60+i0.001
P_{11}
$-P_{12}/P_{11}$
P_{22}/P_{11}
r_{eff}=3.0μm
v_{eff}=12.3
P_{33}/P_{11}
P_{43}/P_{11}
P_{44}/P_{11}
Scattering Angle (°)
Scattering Angle (°)
Scattering Angle (°)

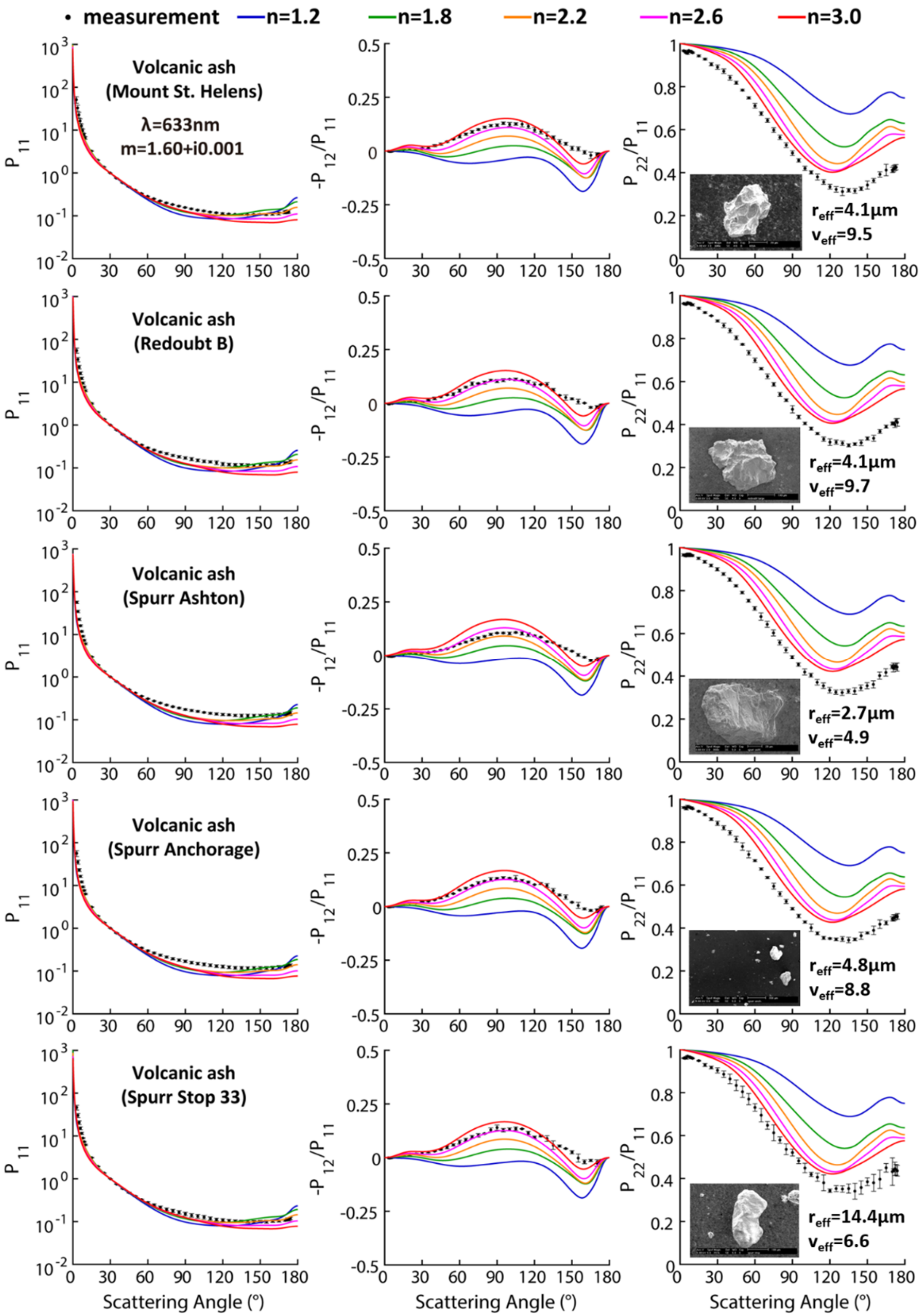

Three key scattering matrix elements (P_{11}, $-P_{12}/P_{11}$, and P_{22}/P_{11}) of simulations and measurements at 632.8nm wavelength for five volcanic ash samples. The refractive index was selected to be 1.60+i0.001 for all the samples.

LiDAR DUST Observations

Filed campaign		time	location
SAMUM (Saharan Mineral Dust Experiment)	SAMUM I	May–June 2006	southern Morocco
	SAMUM-2a	January– February 2008	Cape Verde
	SAMUM-2b	May–June 2008	
SALTRACE-3 (Saharan Aerosol Longrange Transport and Aerosol-Cloud-Interaction Experiment)		June–July 2014	Caribbean island of Barbados
SHADOW campaign (Study of Saharan Dust Over West Africa)		March–April 2015	Senegal
CADEX (Central Asian Dust EXperiment)		March 2015 to August 2016	Dushanbe,Tajikistan

Depolarization ratio observations at different locations

Location	0.355 μm	0.532 μm	1.064 μm	Reference
Midwest	0.246 ± 0.018	0.304 ± 0.005	0.270 ± 0.005	Burton et al. (2015)
Chihuahuan	0.243 ± 0.046	0.373 ± 0.014	0.383 ± 0.006	Burton et al. (2015)
Caribbean	-	0.327 ± 0.018	0.278 ± 0.012	Burton et al. (2015)
Pico de Orizaba	-	0.334 ± 0.018	0.400 ± 0.009	Burton et al. (2015)
Barbados	0.252 ± 0.03	0.28 ± 0.02	0.225 ± 0.02	Haarig et al. (2017)
Ouarzazate	0.28 ± 0.05	0.31 ± 0.03	0.26 ± 0.04	Freudenthaler et al. (2009)
Ouarzazate	0.24 ± 0.07	0.30 ± 0.03	0.27 ± 0.04	Freudenthaler et al. (2009)
Tajikistan	0.18-0.29	0.31-0.35	-	Hofer et al. (2017)
Cape Verde	0.24-0.27	0.29-0.31	-	Groß et al. (2011)
Munich	0.30 ± 0.07	0.34 ± 0.03	-	Wiegner et al. (2011)

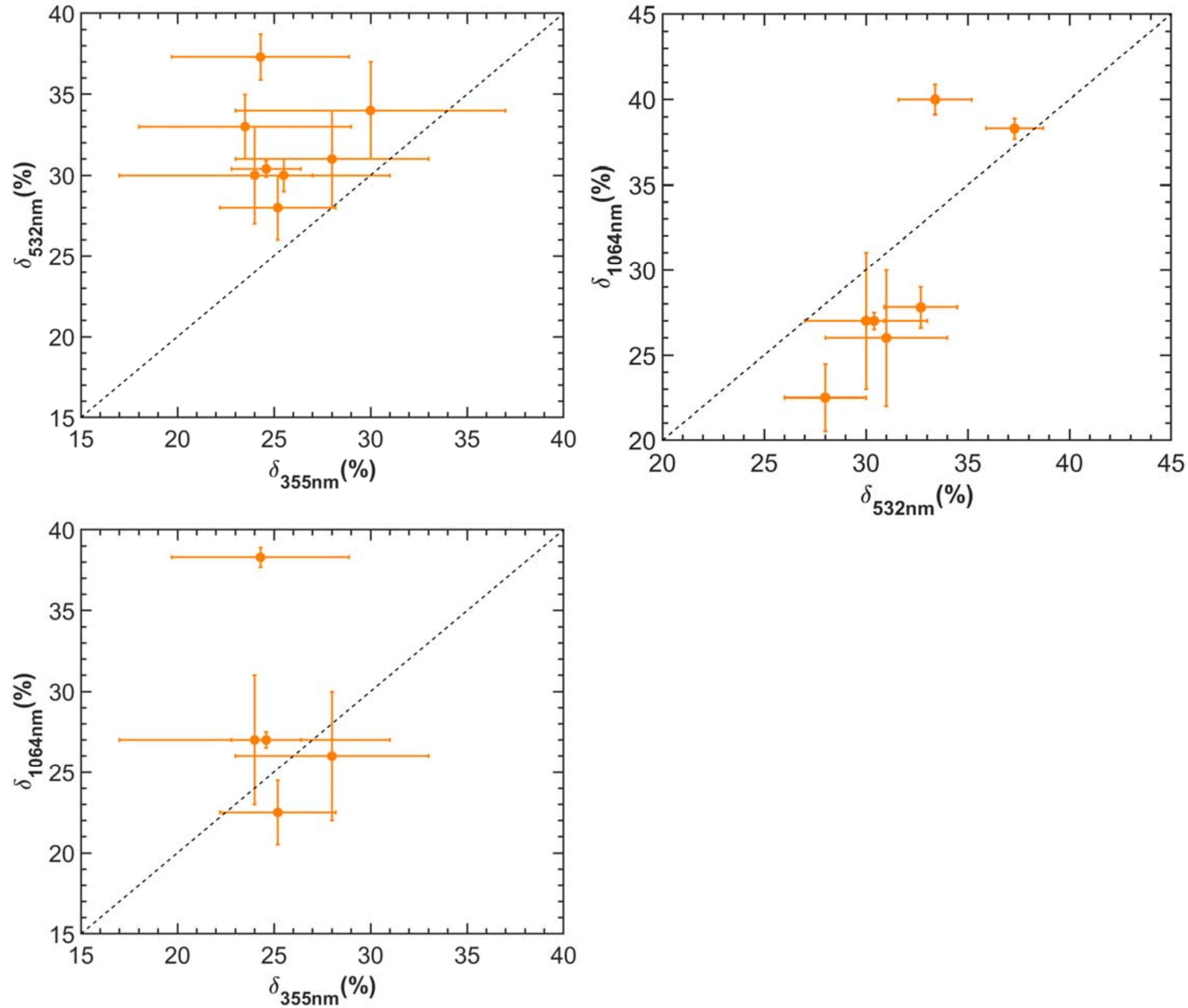

δ532nm(%)
δ355nm(%)
δ1064nm(%)
δ532nm(%)
δ1064nm(%)
δ355nm(%)

LiDAR ratio measurements at Different Locations

Location	0.355 μm	0.532 μm	1.064 μm	Reference
Tajikistan	46.9 ± 2.1	42.9 ± 3.2	-	Hofer et al. (2017)
Cape Verde	58 ± 7	62 ± 5	-	Groß et al. (2011)
Munich	58 ± 13	56 ± 10	-	Wiegner et al. (2011)
Ouarzazate	52.9 ± 7	54.8 ± 6.7	54.9 ± 12.7	Tesche et al. (2009)
Gwangju	56 ± 10	51 ± 6	-	Noh et al. (2008)
Mbour	54 ± 8	53 ± 8	-	Veselovskii et al. (2016)
Gwangju	52 ± 7	53 ± 8	-	Shin et al. (2016)
Portugal	45 ± 8	53 ± 7	-	Preißler et al. (2011)
Barbados	53 ± 5	53 ± 7	-	Groß et al. (2015)
Tokyo	48.6 ± 8.5	43.1 ± 7.0	-	Murayama et al. (2004)
Guangzhou	48.5 ± 7.5	51.7 ± 8.3	-	Heese et al. (2017)

Laboratory Measurements

Scatterring Angle	0.355 μm	0.532 μm	1.064 μm	Reference
178°	0.21 ± 0.02	0.16 ± 0.02	0.09 ± 0.02	Mamouri and Ansmann (2015)
$180 \pm 0.2°$	0.375 ± 0.015	0.350 ± 0.015	-	Miffre et al. (2016)
$180 \pm 0.2°$	0.355 ± 0.015	0.305 ± 0.015	-	Miffre et al. (2016)

Impact of Real Part of the Refractive Index

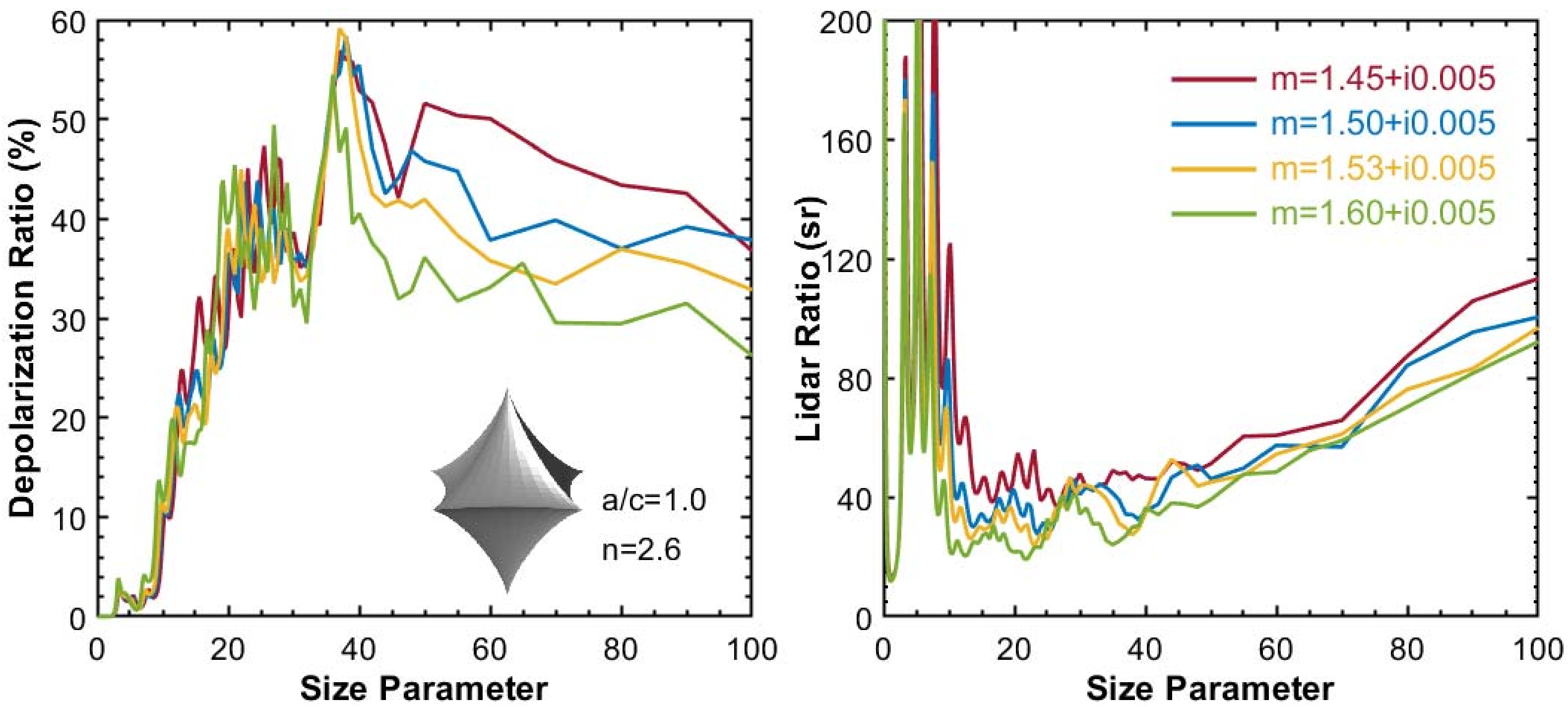

Impact of the Imaginary Part of the Refractive Index

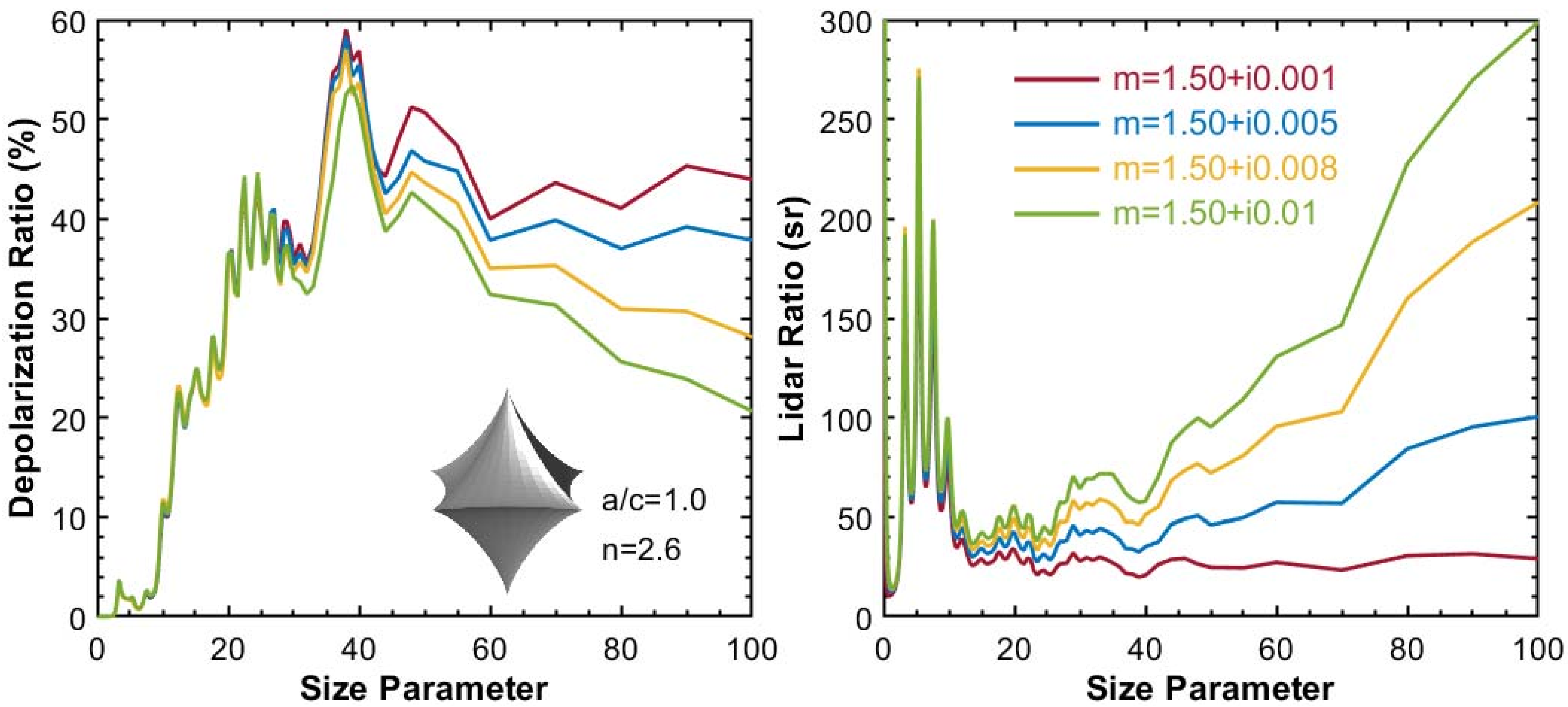

Small sizes

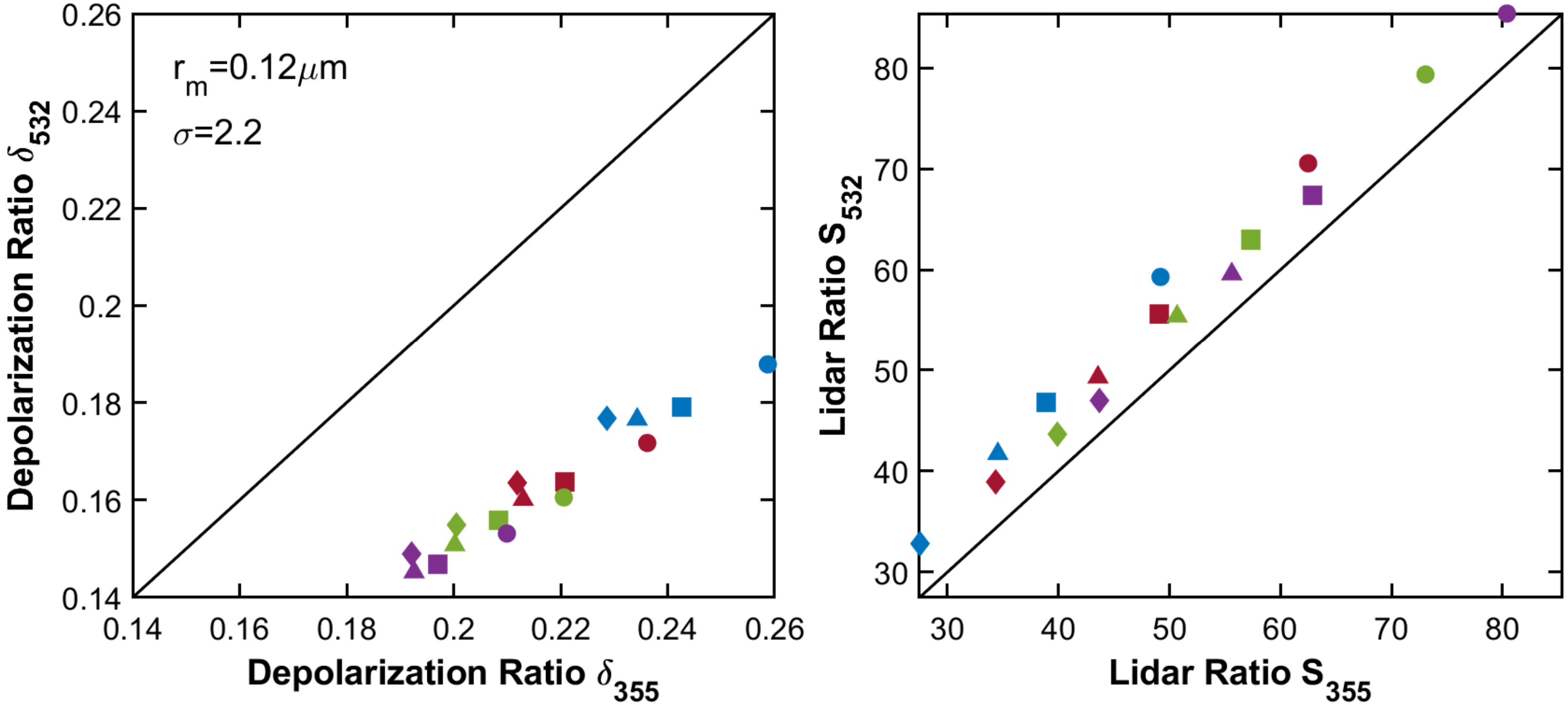

r_m=0.12μm
σ=2.2
Depolarization Ratio δ_{532}
Depolarization Ratio δ_{355}
0.14
0.16
0.18
0.2
0.22
0.24
0.26
Lidar Ratio S_{532}
Lidar Ratio S_{355}
30
40
50
60
70
80

Large sizes

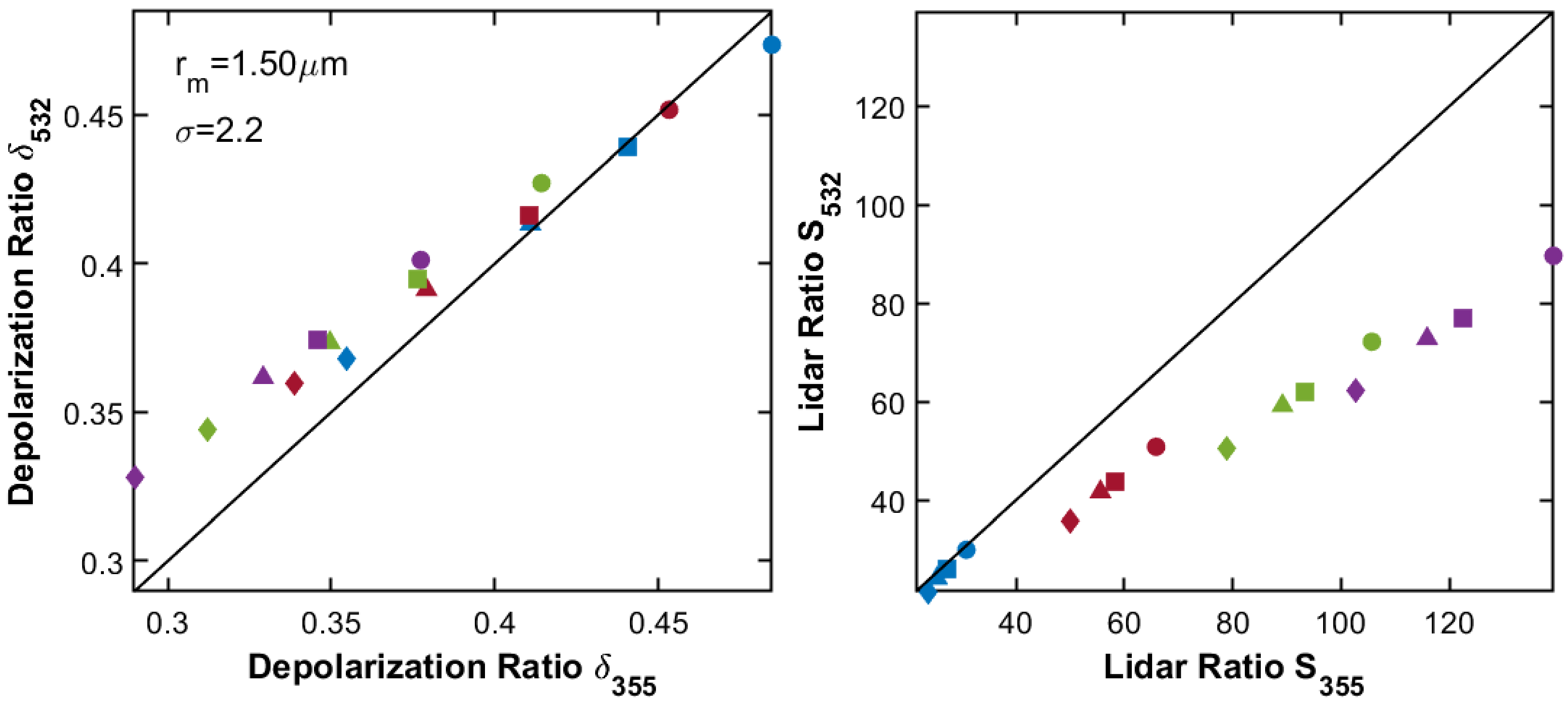

r_m=1.50μm
σ=2.2
Depolarization Ratio δ_{532}
Depolarization Ratio δ_{355}
0.3
0.35
0.4
0.45
Lidar Ratio S_{532}
Lidar Ratio S_{355}
40
60
80
100
120

Fine mode + Coarse mode

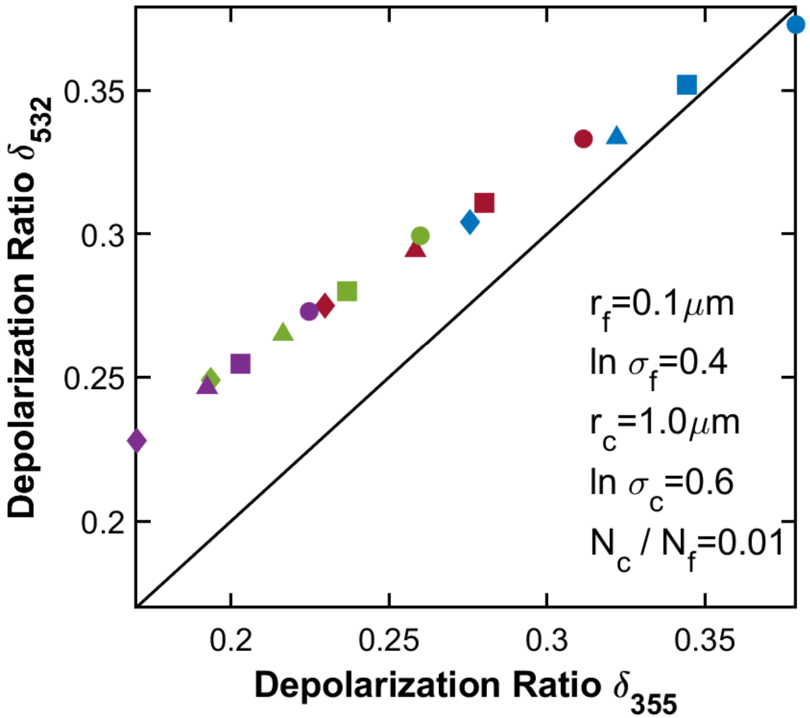

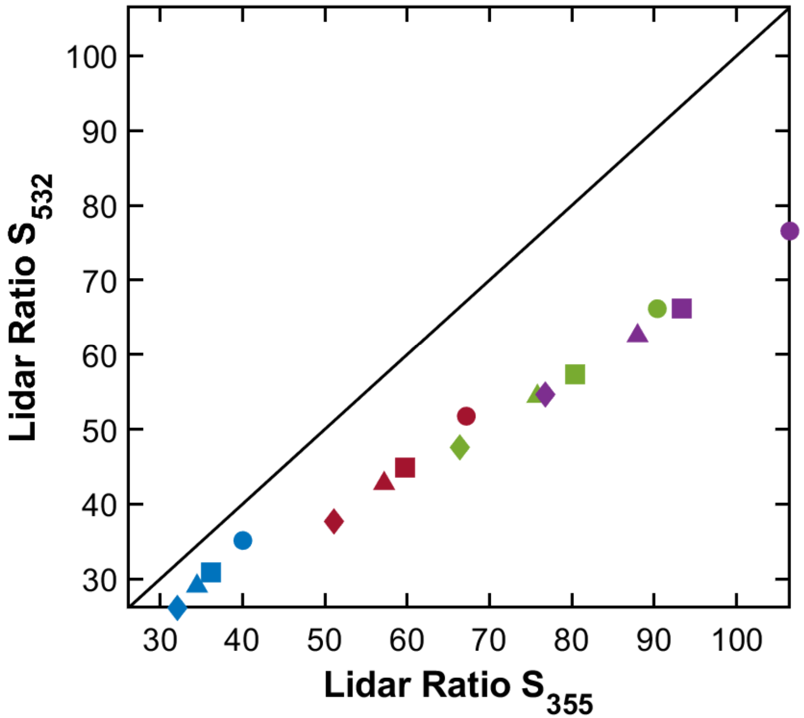

Dust-soot Mixtures

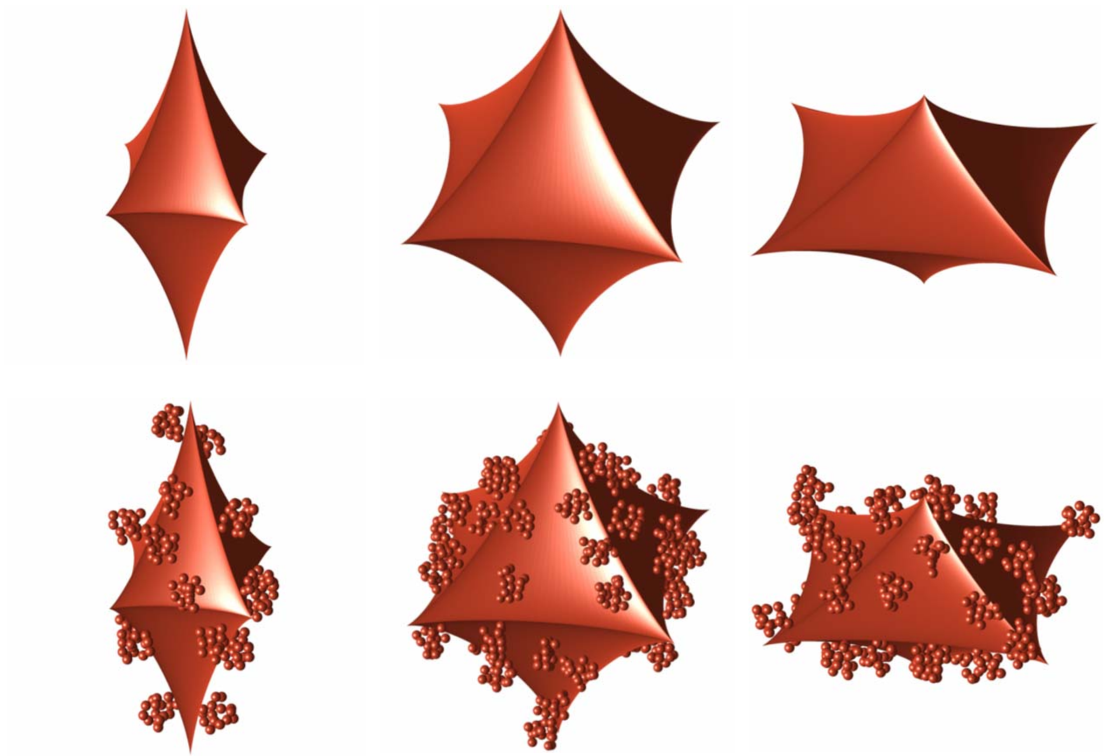

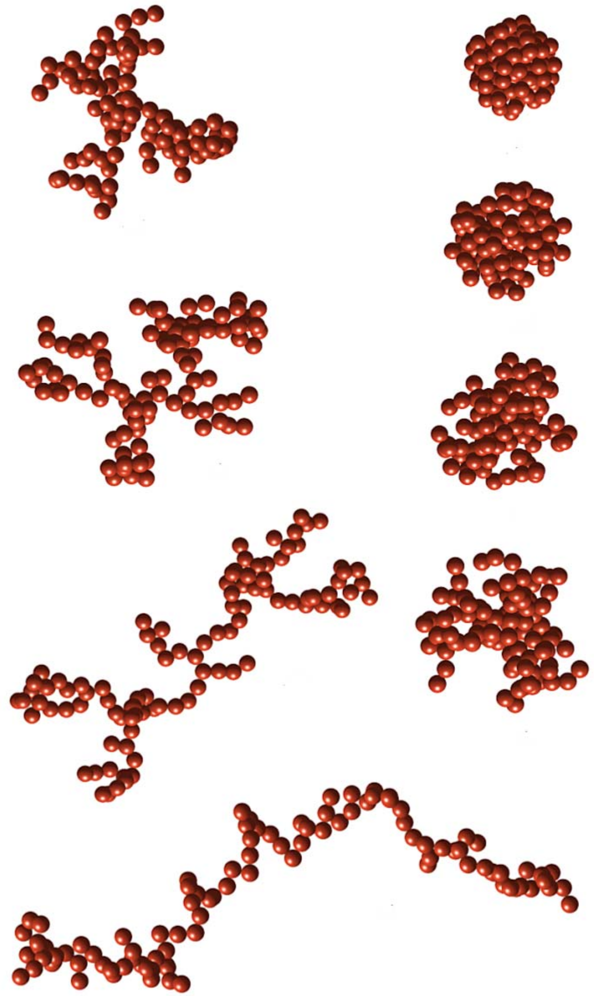

(e.g., Sorenson, 2001)

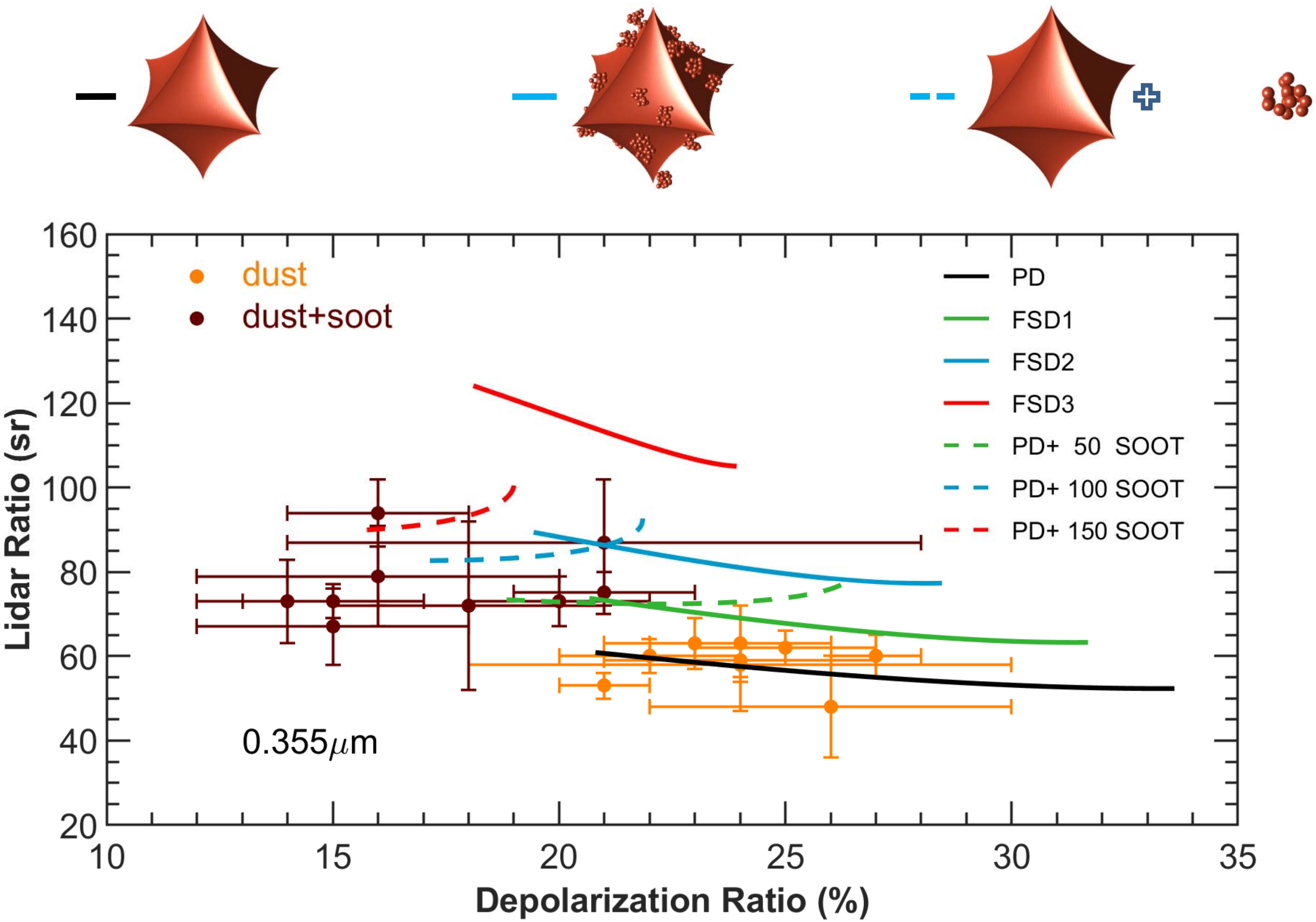

Noncontact mixing is closer to observations.

Sea-salt optical modeling

Schematic of Sea-spray Aerosol Production

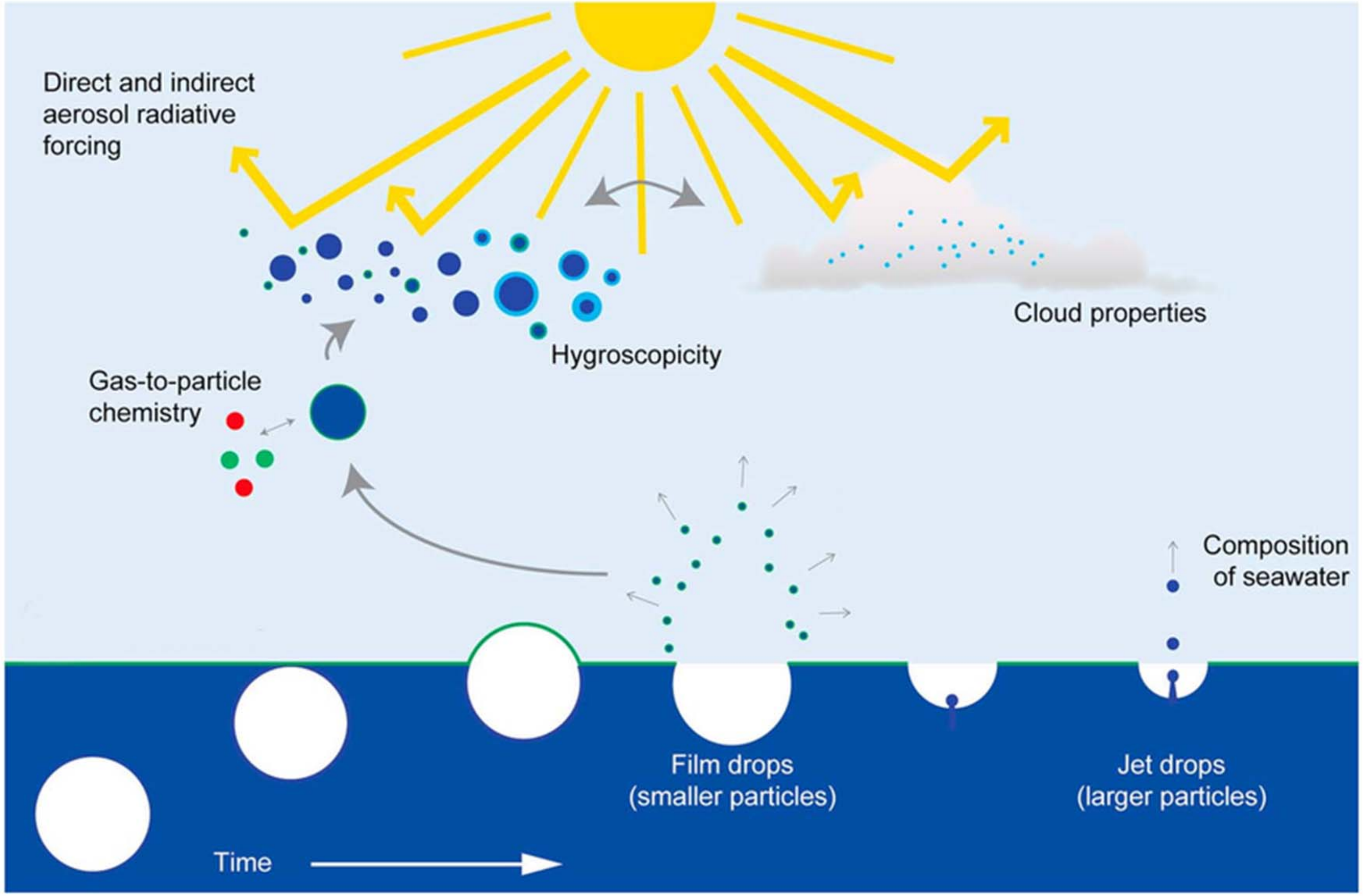

(After Salter, Matthew E., et al *Geophysical Research Letters* 2016)

Dry sodium choride

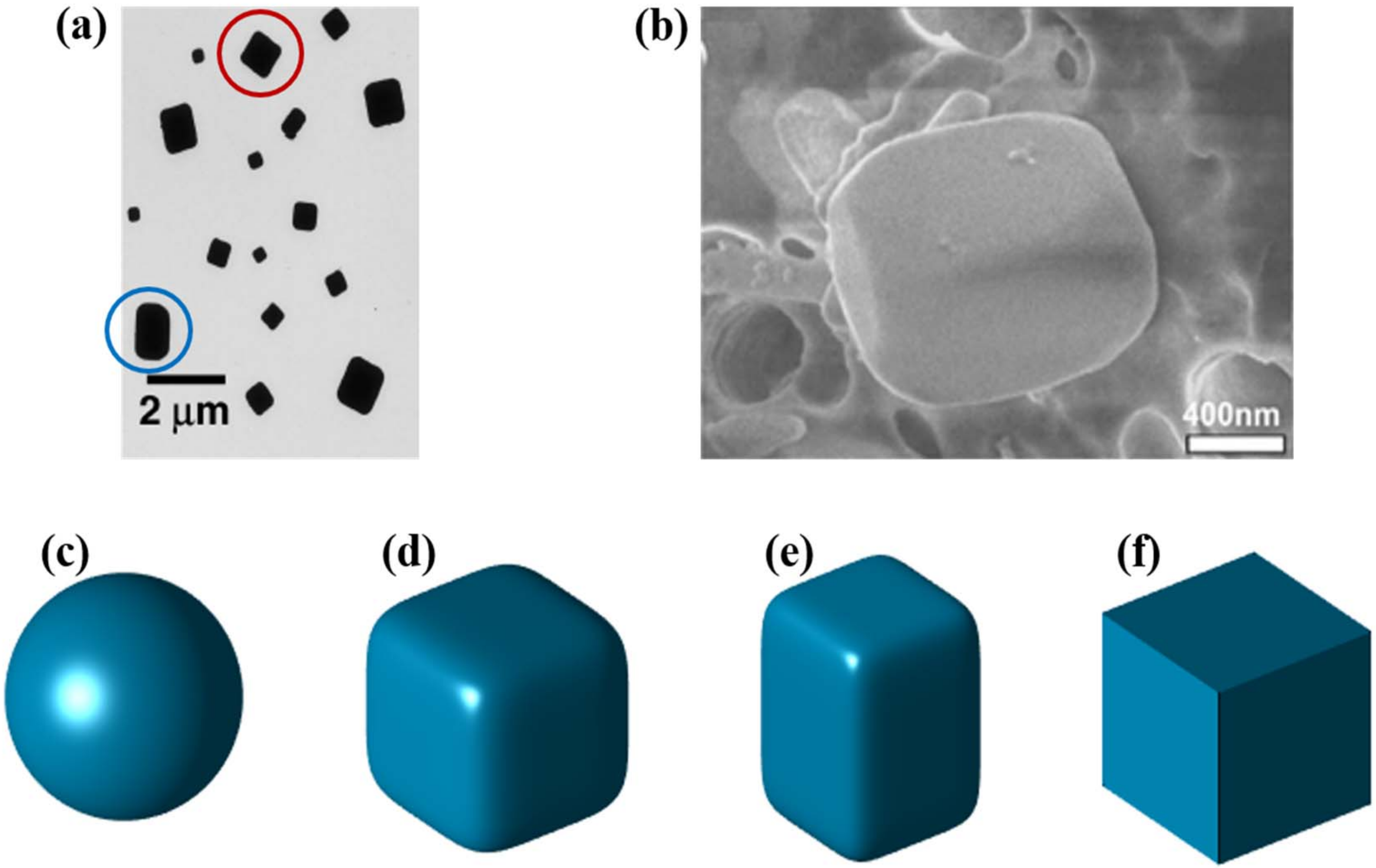

Aspect Ratio and Roundness Effect

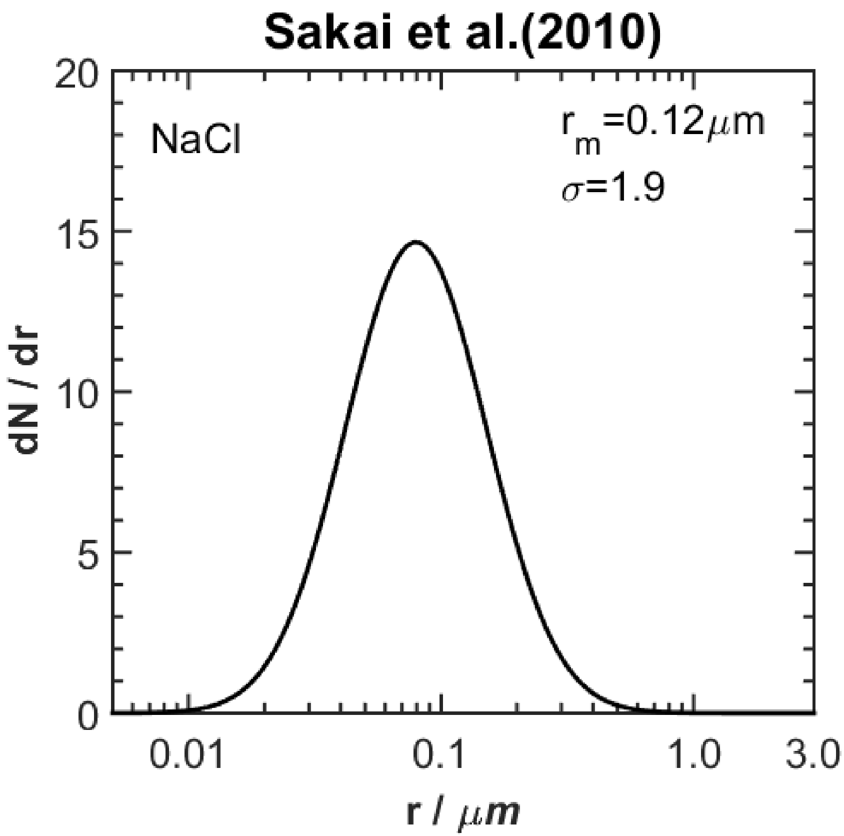

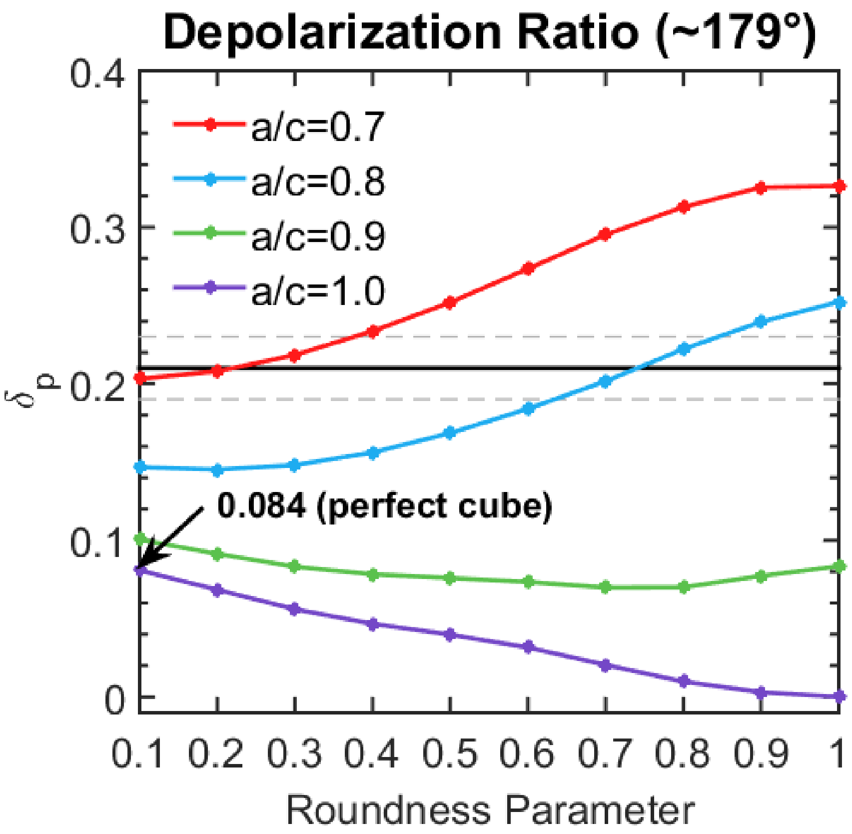

Wet Sea Salt Aerosols

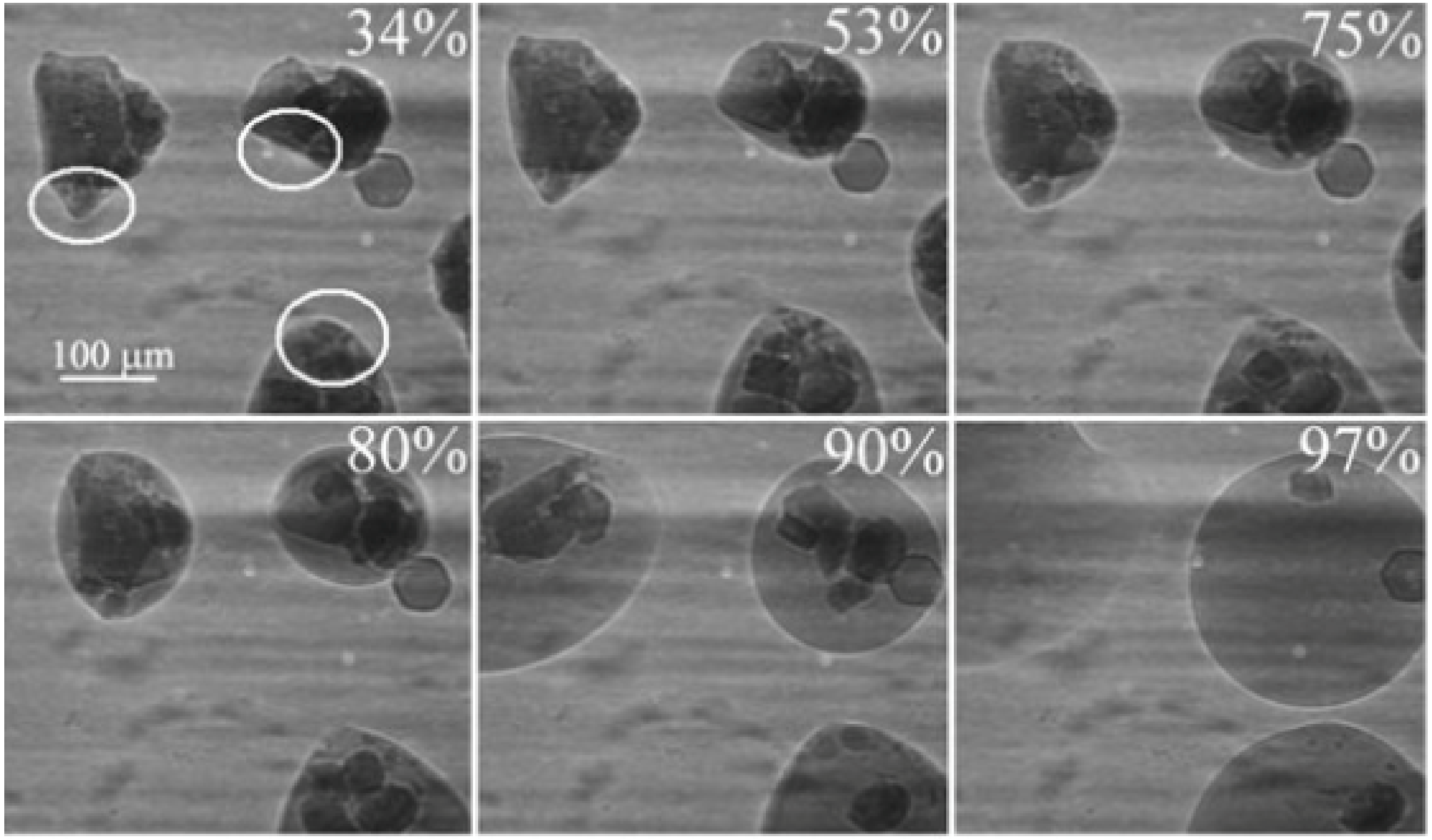

X-Ray phasing technique(Zeng et al. 2012)

Depolarization VS Relative Humidity

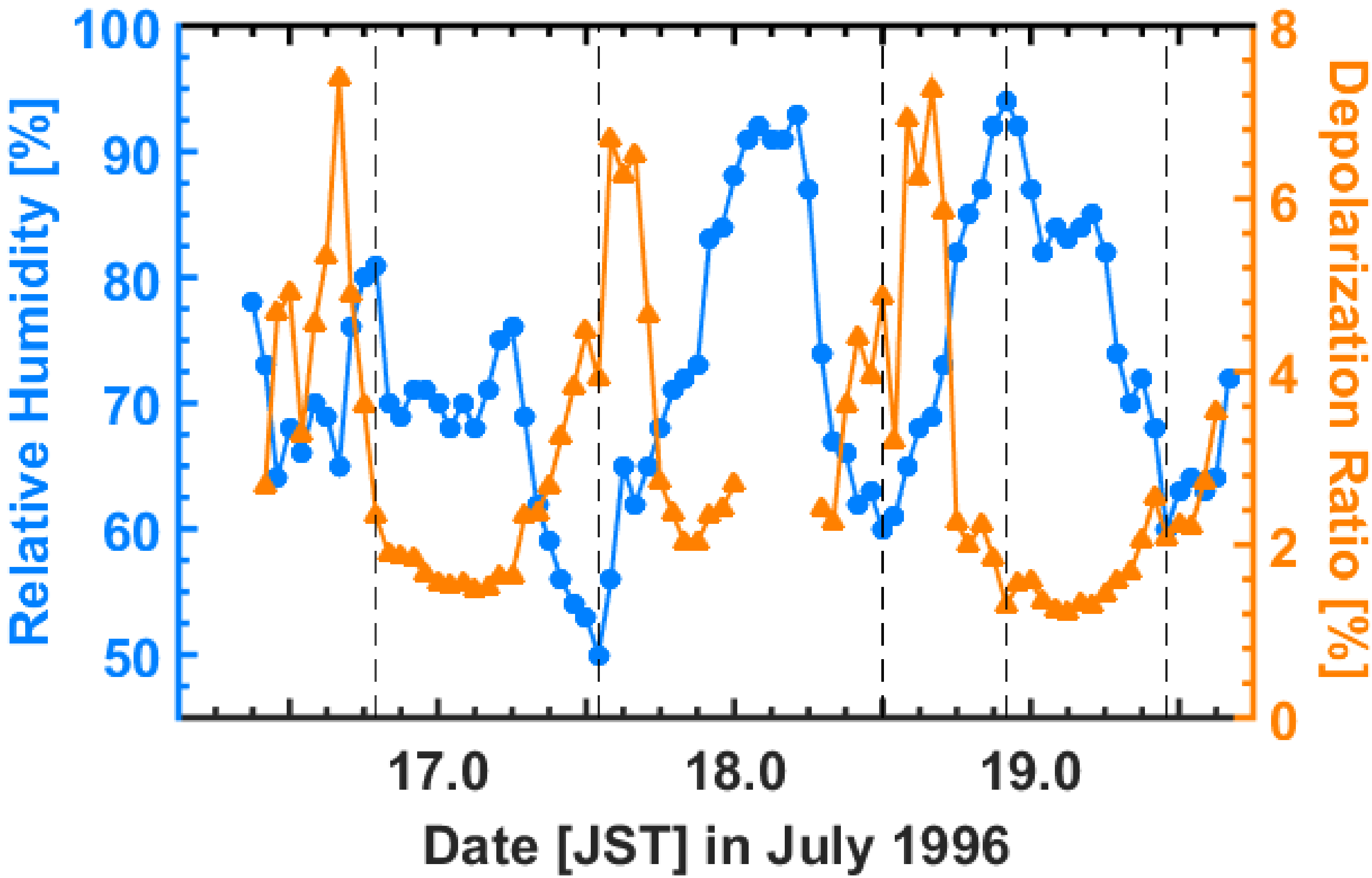

Data from Toshiyuki Murayama

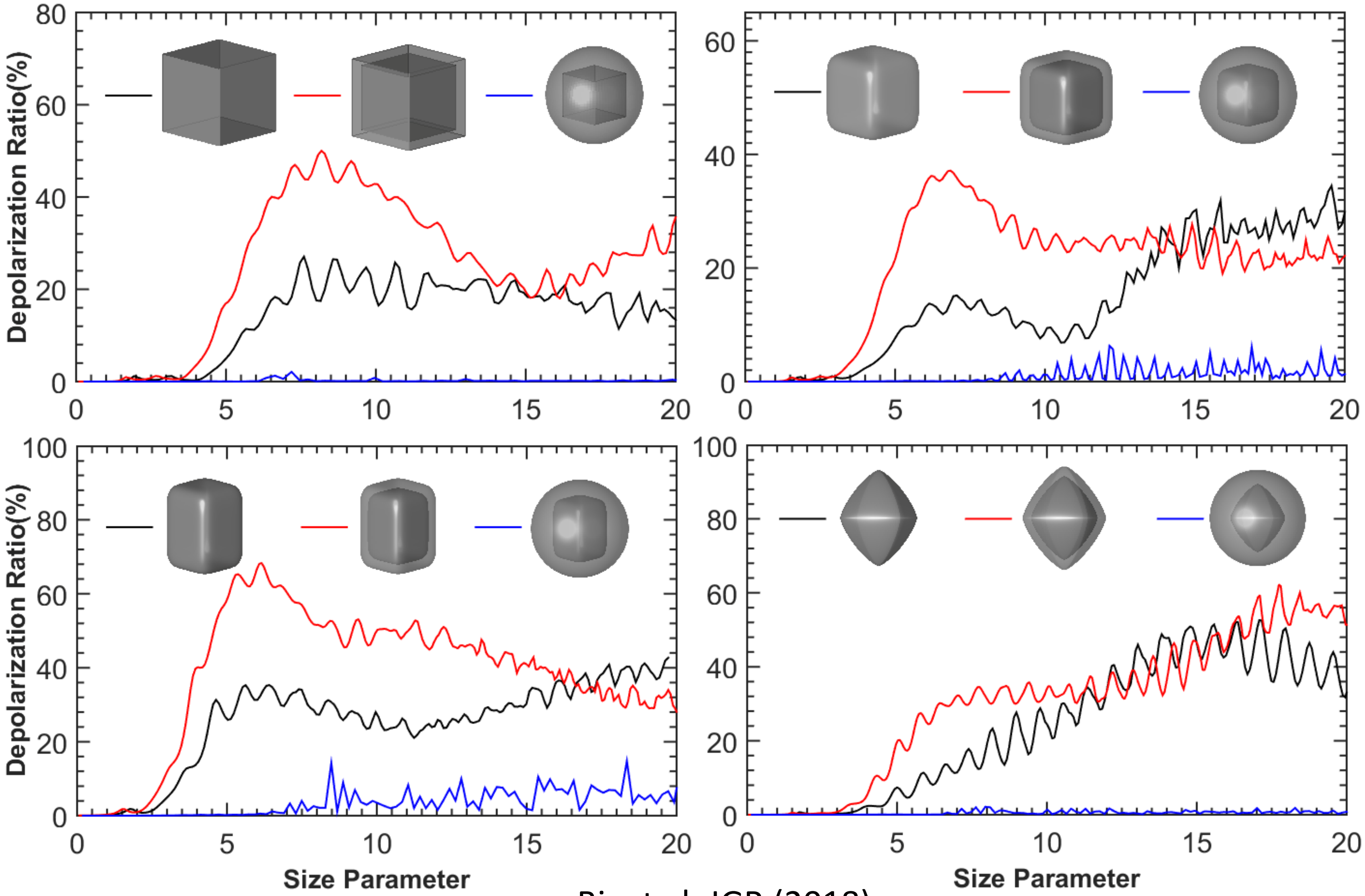

Bi, et al. JGR (2018)

Effect of Particle Inhomogeneity (RH=50~80% inhomogeneous)

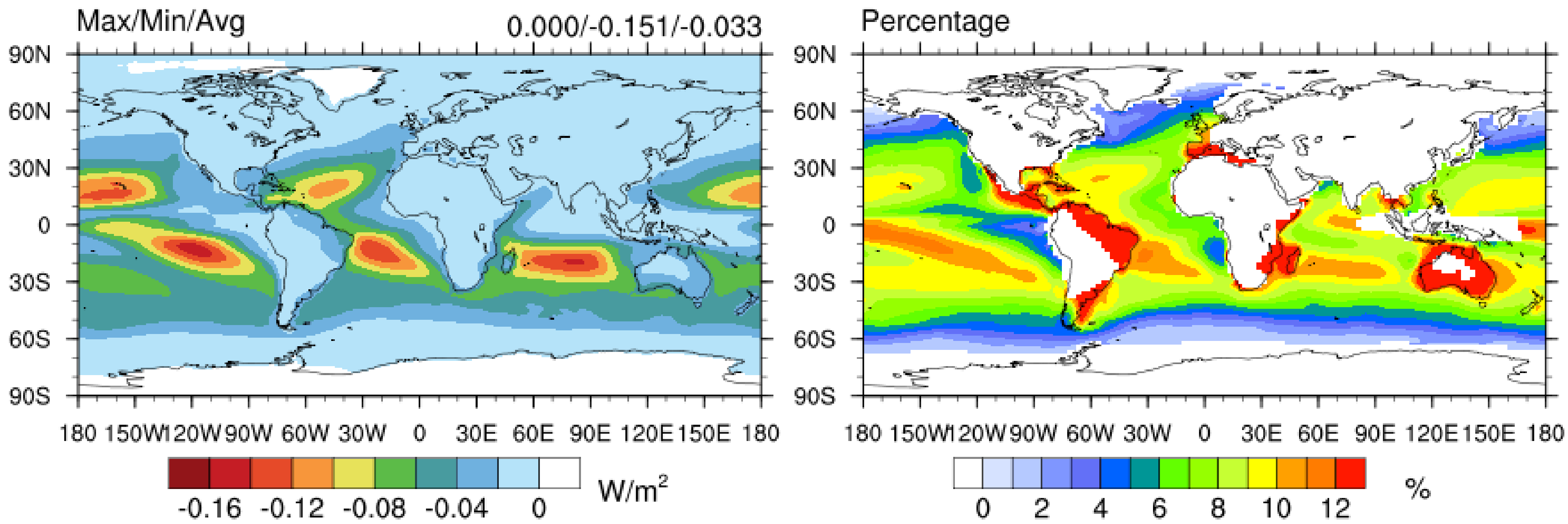

difference

difference/forcing (forcing > 0.1 Wm^{-2})

Global mean: 0.033/0.408 = 8%

Wang, et al. GRL (2019)

Summary

- Significant progress has been made on computing the optical properties of non-spherical particles. Extensive computations are now allowable with reasonable computational resources and computational time.
- Comparison with measurement and observations show that super-ellipsoidal space is quite promising with applications in remote sensing and radiative transfer modeling.

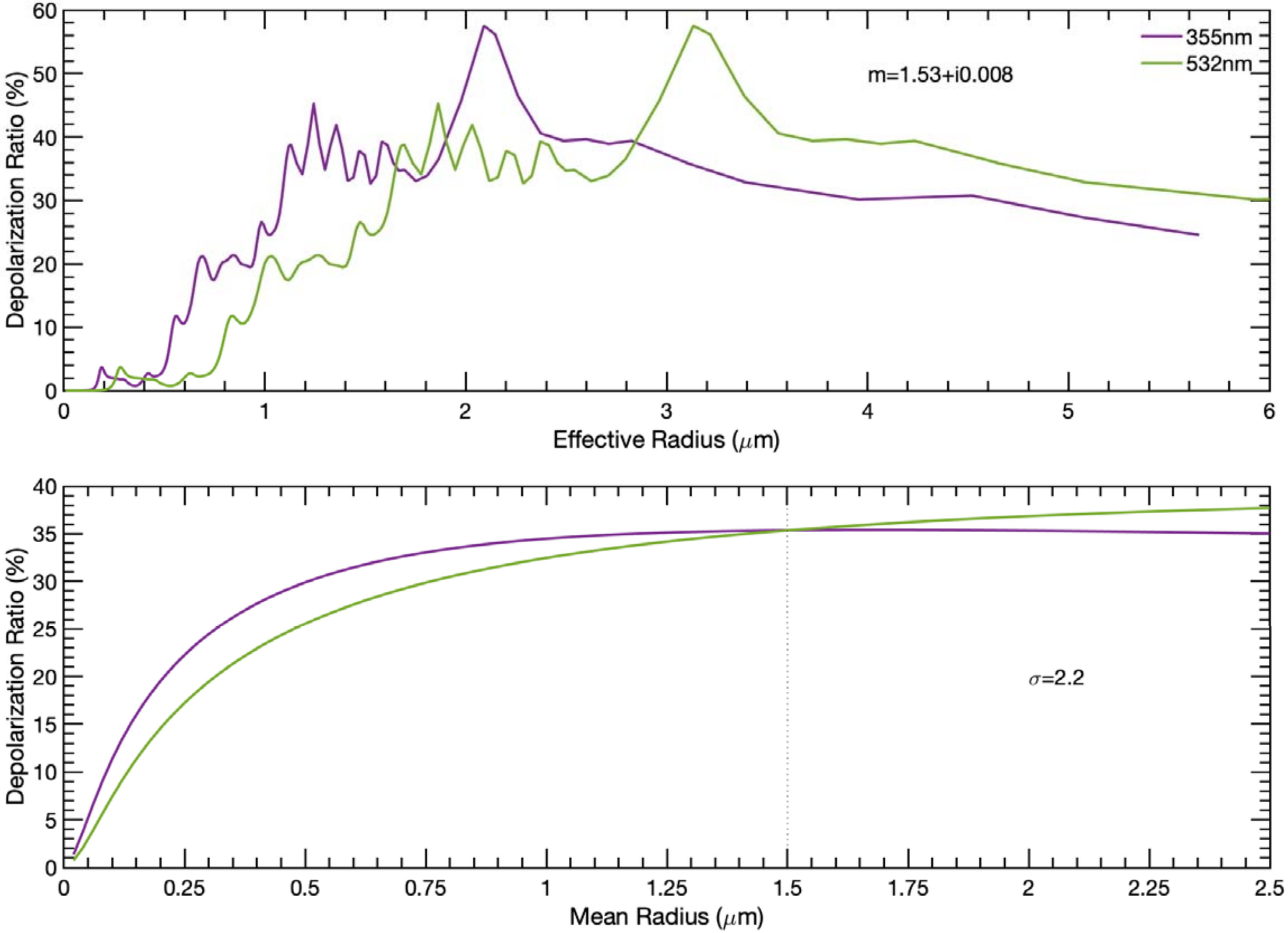

355nm
532nm
m=1.53+i0.008
Depolarization Ratio (%)
Effective Radius (μm)
σ=2.2
Depolarization Ratio (%)
Mean Radius (μm)

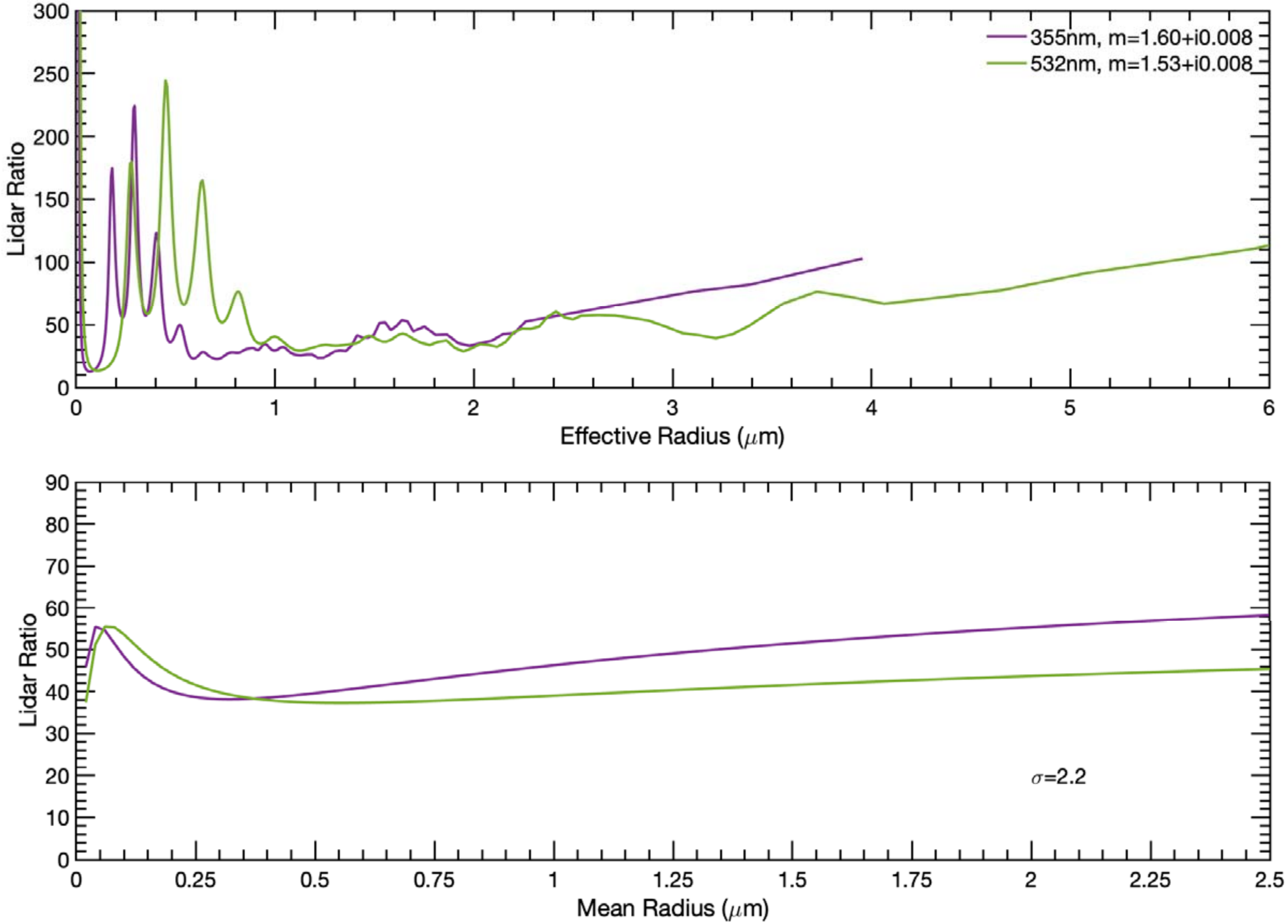

355nm, m=1.60+i0.008
532nm, m=1.53+i0.008
Lidar Ratio
Effective Radius (μm)
Lidar Ratio
σ=2.2
Mean Radius (μm)

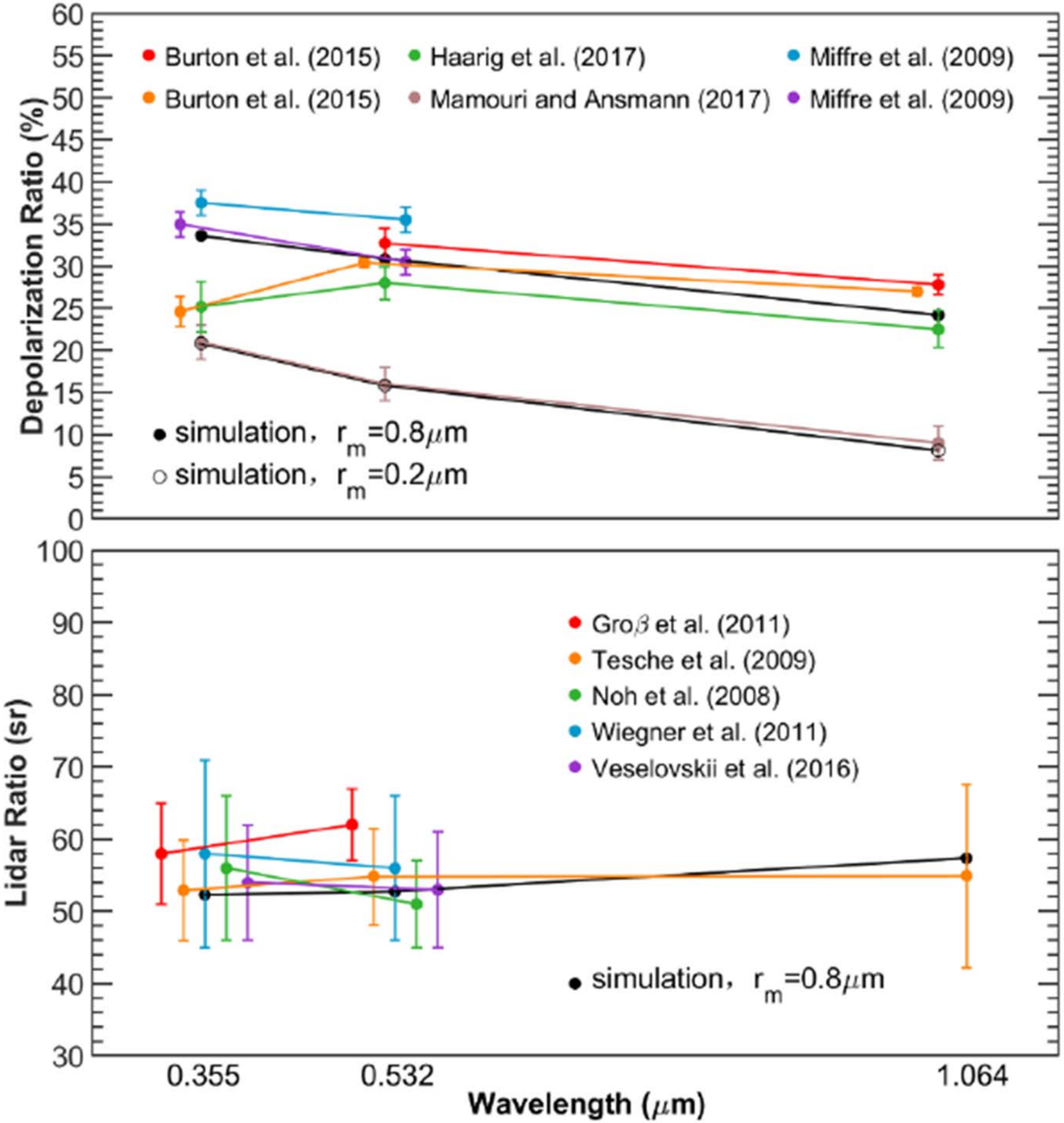

Tang et al., Optics Express,(2019)

Polarization Simulations

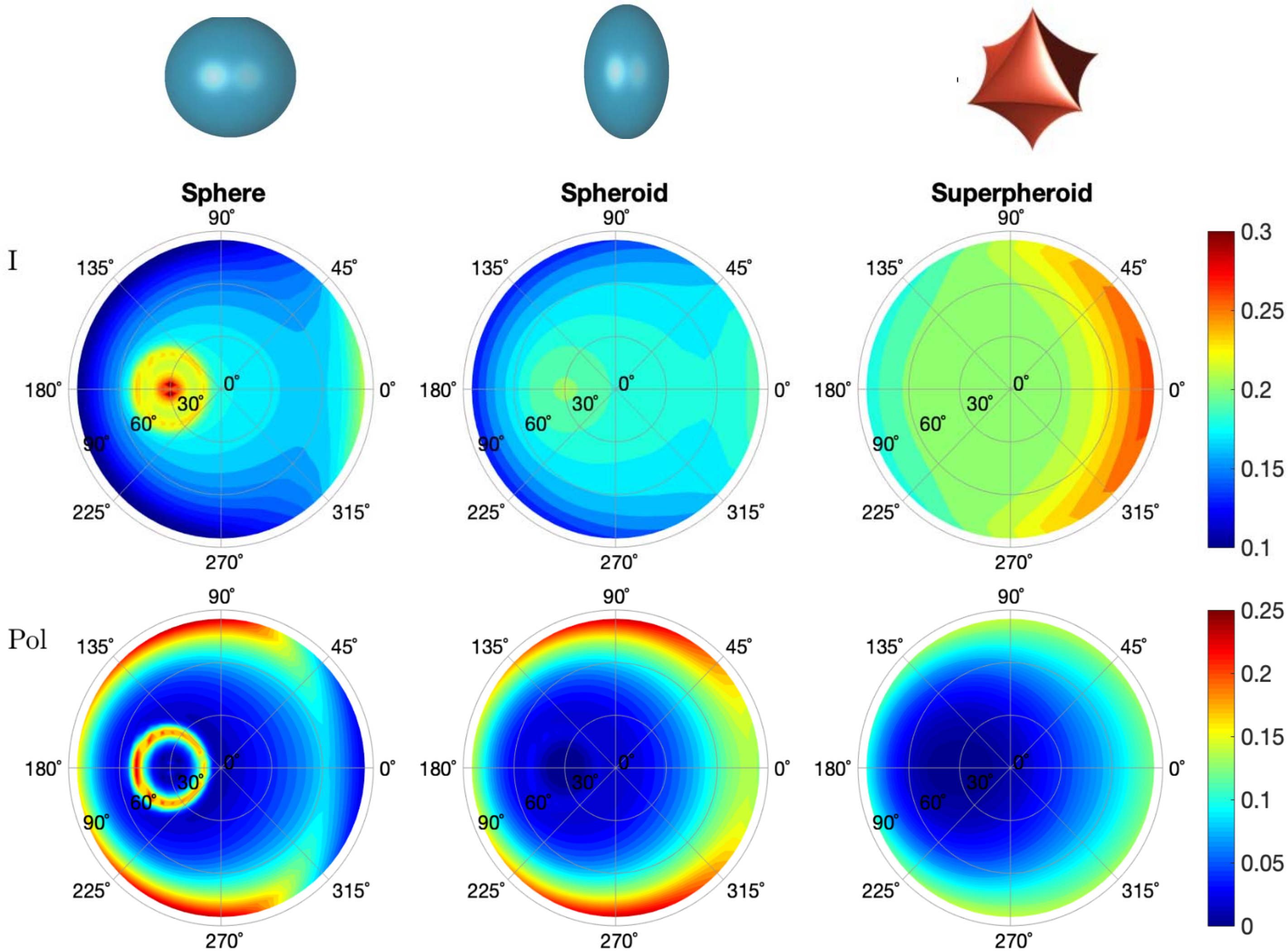

Dry sea salt

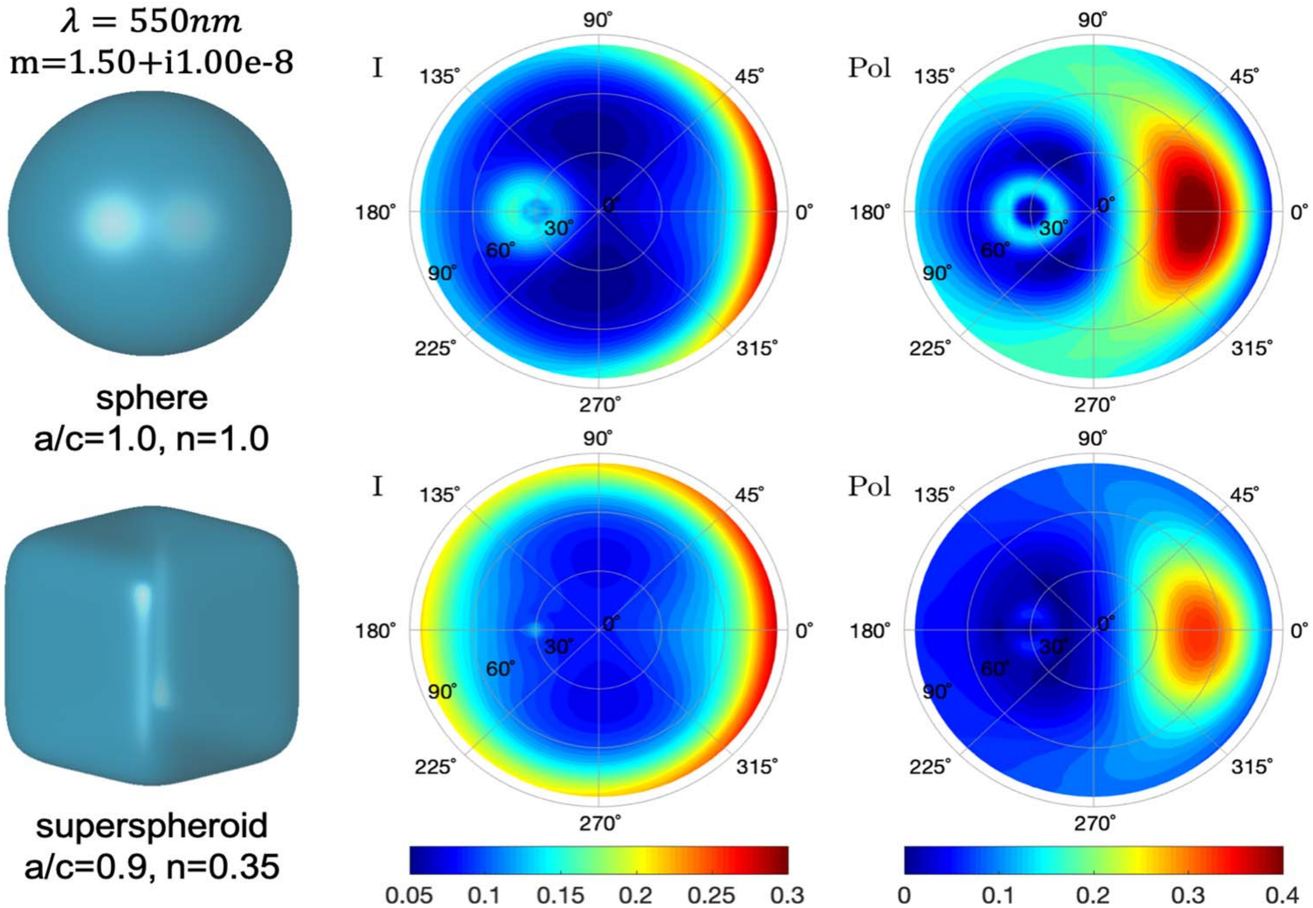
$\lambda = 550nm$
m=1.50+i1.00e-8
sphere
a/c=1.0, n=1.0
superspheroid
a/c=0.9, n=0.35
I
Pol
90°
45°
0°
315°
270°
225°
180°
135°
0°
30°
60°
90°
0.05
0.1
0.15
0.2
0.25
0.3
0
0.1
0.2
0.3
0.4

Wet sea salt

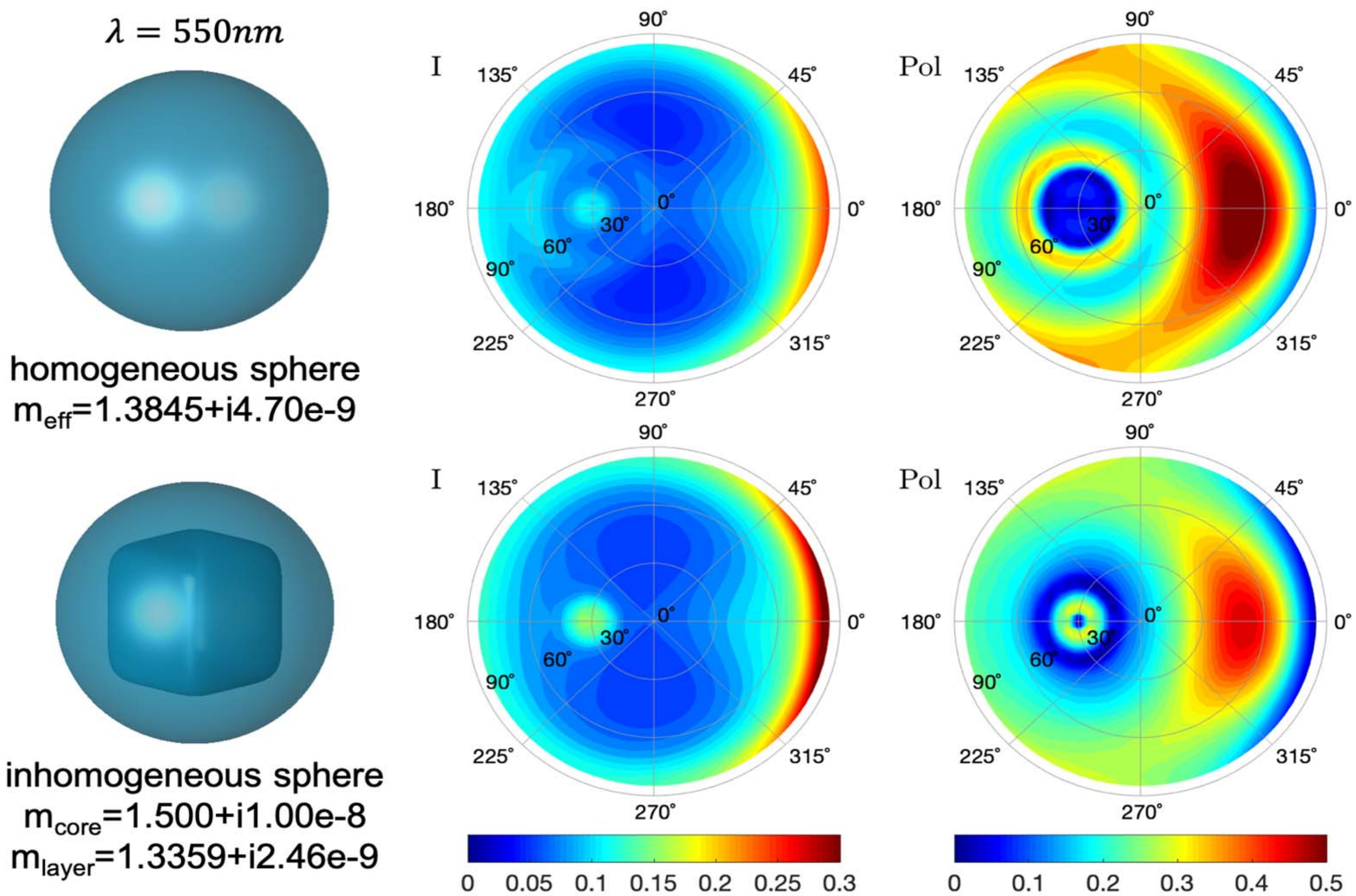

λ = 550nm
homogeneous sphere
m_eff=1.3845+i4.70e-9
inhomogeneous sphere
m_core=1.500+i1.00e-8
m_layer=1.3359+i2.46e-9
I
Pol
90° 135° 45° 180° 0° 225° 315° 270°
0° 30° 60° 90°
0 0.05 0.1 0.15 0.2 0.25 0.3
0 0.1 0.2 0.3 0.4 0.5